RT NO. 6 - GALCIT 101
Thiokol Subcontract No. R 69752
January 1, 1960 - May 31, 1960

FUNDAMENTAL STUDIES RELATING TO SYSTEMS ANALYSIS OF SOLID PROPELLANTS

15 June 1960

Guggenheim Aeronautical Laboratory
California Institute of Technology
Pasadena, California

PROGRESS REPORT NO. 6 -GALCIT 101

Subcontract No. R-69752

January 1, 1960 - May 31, 1960

Fundamental Studies Relating to Systems Analysis of Solid Propellants

P. J. Blatz
W. G. Knauss
R. A. Schapery
M. L. Williams

This research is supported by
The Thiokol Chemical Corp., Redstone Division

Guggenheim Aeronautical Laboratory
California Institute of Technology
Pasadena, California

PREFACE

Previous reports of this series have attempted to define some of the important parameters affecting structural integrity of solid propellant rocket grains. Three general areas have been discussed, namely material properties, analytical procedures, and criteria for mechanical failure.

This particular report is devoted to failure criteria, including both limiting deformation and fracture. First of all, the characteristic material properties of filled and unfilled elastomers are described, followed by a brief description of current and proposed tests which can be conducted to obtain experimental information relating to these characteristics in such a form that they can be incorporated in structural integrity analyses. In particular, the necessity for multi-axial tests is stressed in conjunction with minor requirements for new experimental equipment.

The selection of appropriate fracture criteria is discussed. Most progress, however, can be reported only in criteria for unfilled elastomers for small and large strains where it appears a distortion strain energy density may be used. It is necessary to delay any really definitive remarks upon filled elastomers or actual grain composites, and subsequent use with cumulative damage analyses, until additional experimental data for propellants is forthcoming.

TABLE OF CONTENTS

TABLE OF CONTENTS (Cont'd)

TABLE OF CONTENTS (Cont'd)

V. FAILURE ANALYSIS

A. Common Types of Failure Criteria

It has been repeatedly emphasized in earlier reports [1-5] that a complete analysis of the structural behavior of a solid propellant rocket motor includes not only a stress or strain analysis, but also a failure analysis. Previous reports have aimed primarily at investigating methods of estimating the stresses or strains in a viscoelastic propellant material due to prescribed applied loads. In this report, we propose to treat the companion problem of predicting the maximum imposed loading at which either excessive deformation or fracture threshhold is reached.

1. Deformation criteria

As implied in the foregoing there are usually two basic structural engineering criteria, deformation and fracture. By way of example in solid propellant applications, they are exemplified by slump and grain cracking, respectively. Generally the first of these is tied in rather closely with ballistic performance and storage procedures, that is to say a maximum permissible deformation without fracture is more or less arbitrarily prescribed. If this is the case, it becomes a simple matter to complete the analysis by finding the loading or time corresponding to that state when this deformation is reached by applying the viscoelastic analysis techniques previously developed.

One illustration is the situation wherein a second stage rocket grain may be fired vertically and subjected to inertia loading for short periods, say, of the order of minutes. On the other hand, the grain, perhaps for logistic reasons, may be stored vertically for extended periods and in this condition also subjected to vertical gravity forces but over a considerably longer time. Both of these situations require the prediction of time dependent deformations—the first under $\underline{n} \cdot \underline{g}$ gravity loading for short time, the second for one $\underline{g}$ loads over long time.

The elastic analysis for such a condition has been presented in the third report of this series wherein it is shown that the inward radial constri ction of a thick walled case-bonded cylindrical grain at the base depends upon the

support conditions. If the base is completely unsupported, the throat area does not choke at all but takes up the general deformation pattern shown in the sketch. On the other hand, if the base is rigidly supported, there will be a choking tendency as shown. Its magnitude, in the particular

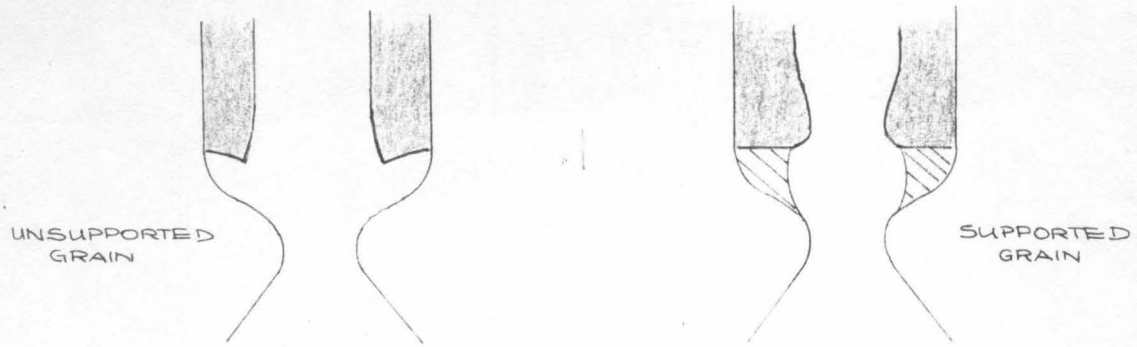

case where the web fraction was fifty percent, was found to be of the order

$$\frac{\Delta a}{a} \approx 20 \frac{\rho b n}{E}$$

where ρ is the density (pci) of the propellant and n the number of times gravity load. To examine the effect upon ballistic performance one could compute the relative change in port area $\Delta A_p / A_p$ to be twice the above figure. The previous calculation is based upon an elastic analysis, when E is the elastic modulus. An approximation to the time dependent deformation can be obtained by replacing E by its viscoelastic equivalent, which for a three element model gives

$$\frac{\Delta A_p}{A_p} \approx \frac{40 \rho b n}{m_e} \left[1 - \left(1 - \frac{m_e}{m_g} \right) e^{- \frac{m_e}{m_g} \frac{t}{\tau}} \right]$$

where it may be easily checked that for long times $E \to m_e$, the rubbery modulus, and for short times $E \to m_g$, the glassy modulus. The relative amount of choking is seen to depend upon the mechanical properties, including the characteristic relaxation time. If therefore the maximum permissible blockage were specified as the design criterion, one could compute the time at which it would be exceeded for a given gravity load. A reasonably large grain, for example, would have an upper bound of approximately ten percent per g at room temperature.

The analysis given is approximate, but is presented to make the point that if a deformation criterion is imposed, it is merely necessary to refine the appropriate deformation analysis to the accuracy desired for the prediction. As the procedure is straight forward, although not necessarily simple in a given problem because the strain analysis itself is complicated, no additional remarks upon the deformation criterion will be included at this time.

2. Fracture criteria

In contrast to deformation, the mechanics of fracture requires a fundamentally different type of investigation. Fracture first occurs on the microscopic scale, when the medium is non-continuous. Hence the analysis techniques, based as they are upon the assumption of a macroscopic continuum, are not valid at the point of fracture. For this reason the problem of fracture analysis is markedly more complicated inasmuch as it requires a knowledge of molecular behavior not smoothed out by the macroscopic averaging process. On the other hand, it has proven possible to determine certain extremely useful gross fracture characteristics, for example uniaxial tensile strength as a function of strain rate and temperature. From the engineering standpoint, it is desirable to extend, empirically if necessary, such limited information on special test samples to more complex geometries such as a star grain.

The general requirement for such a correlation is by no means new, although a precise statement for viscoelastic materials has not been particularly emphasized. Nadai[6] enumerates for example several different fracture criteria, primarily as used in the study of metals, and it is worth restating them here. Each criterion defines some particular functional of the stress field or strain field, the value of which is to be determined empirically. (As yet molecular theories of strength are not advanced to the point of calculating such numbers theoretically.) When the appropriate functional is exceeded, yield, rupture, fracture or what have you takes place. Seven criteria are listed below:

a) the maximum principal stress

b) the maximum principal strain

c) the maximum stress difference (or shear stress)

d) the maximum strain difference (or shear strain)

e) the maximum total strain energy

f) the maximum distortional strain energy

g) the maximum conserved distortional strain energy

Criteria (a) and (b) refer to the fact that, when three principal stresses are acting along principal axes of the stress or strain ellipsoid, one of them will be a maximum relative to the other two, barring the case of hydrostatic stress. In simple and biaxial tensile fields, these functionals are identical with the yield or ultimate stresses and strains for these fields respectively.

Criteria (c) and (d) stem from the observation that many materials, particularly those which evince ductile fracture (sometimes known as shear fracture) do so along a pair of planes or a cone lying in the direction of greatest shear. The maximum shear stress has the value $\frac{1}{2}(\sigma_1 - \sigma_3)$ and is obtained on a plane inclined 45° to the direction of the principal normal stresses. It is interesting to observe that finite elastic theory predicts an angle greater than 45°, whereas, in fact, a value less than 45° is usually observed. This criterion is not suitable for mathematical formulation since it is necessary to determine first the maximum or minimum stresses (or strains).

An alternate criterion based on a mean value of the stress differences was proposed by von Mises[7]. This takes the form

$$\sqrt{2}\,\sigma_0 = \sqrt{(\sigma_1 - \sigma_2)^2 + (\sigma_2 - \sigma_3)^2 + (\sigma_3 - \sigma_1)^2}$$

and is termed herein the mean deviatoric stress. For both simple uniaxial tension and biaxial tension σ_0 is identical with the yield or fracture stress. For pure shear on the other hand, the yield stress turns out to be $\sigma_0/\sqrt{3}$.

The mean deviatoric stress (or strain) has not been listed as a separate criterion because it is actually related to the distortional strain energy criterion proposed by Huber and Hencky.[8] They observe that

$$W_d = \frac{\sigma_0^2}{6\mu} = \frac{(\sigma_1 - \sigma_2)^2 + (\sigma_2 - \sigma_3)^2 + (\sigma_3 - \sigma_1)^2}{12\mu}$$

The mean deviatoric stress is also $3/\sqrt{2}$ times a quantity known as the octahedral shear stress . The total strain energy listed under (e) was proposed by Beltrami and Haigh [9]. It does not prove satisfactory, since there is no correlation between behavior in pure shear and in pure hydrostatic compression. The conserved distortional strain energy refers to the energy stored in a viscoelastic or plastic material, i.e., over and above what has been dissipated. The theory of application of this criterion is still not in a satisfactory state.

The important point to note is that no universal fracture criterion has been established, and that the success of a given fracture hypothesis depends in large measure upon the material with which it is associated. Inasmuch as no exhaustive investigation of fracture criteria for elastomers has been reported to the authors' knowledge, it would appear that one direct engineering approach is to examine test data in conjunction with certain of the aforementioned criteria, and inquire if any of them give reasonable correlation.

The following paragraphs therefore will present a summary and discussion of some current and proposed tests and their correlation, after a restatement of some of the germane characteristics of elastomers.

B. Material Characteristics of Amorphous Elastomers

A composite solid propellant is a highly filled rubber. Ballistic missile logistics demand that the filler be oxidatively energetic in order to deliver at least 250 sec. of specific impulse in combustion with the binder. The science of propellant chemistry has narrowed down the inventory of such useful oxidizers to the combination ammonium perchlorate-aluminum. In this combination the aluminum fuel serves to prevent over-oxidation of the rubber fuel, and at the same time, by virtue of its high exothermic heat of combustion, overcomes the disadvantage imparted to the exhaust gas by its high molecular weights.

Rheological studies have shown that it is expedient to incorporate the filler as a trimodally distributed agglomerate of particles, ranging from one to 250 microns in diameter with the mean size occurring at about 30 microns. Single crystal studies have shown that the aluminum-rubber bond in tension is approximately 90 psi, and that of the oxidizer rubber about 30 psi. Since the tensile strength of a filled rubber lies in the range 20 to 200 psi at room temperature, it is seen that the filler-binder interaction contributes an important feature to the mechanical behavior of such composites. Because of its relatively high bulk and shear moduli, the filler may be assumed to be absolutely rigid.

The binder, according to current standards, is a synthetic rubber, negligibly crystalline, with a molecular weight between juncture points anywhere from 10 to 100,000. These juncture points may be branch-points at which a tri- or tetra-functional monomer has been incorporated into a condensation polymerization system; or they may be crosslinks effected, not by vulcanization, but by mixed condensation-addition polymerization. The mechanical properties of the binder, without its filler, are not the same as those of the pure rubber. The polymerization process is markedly affected by the presence of the filler.

Needless to say, the mechanical properties of such a composite are a quite complicated function of the properties of the binder, of the volume fraction, particle size distribution, and adhesion of the filler. In order to understand the fracture mechanics of such a system, it is appropriate to

study first the fracture mechanics of unfilled rubbers, and then study the modifications produced by various degrees of filler. In carrying out this comparison, it is extremely important to remember that the filler not only modifies the mechanical properties, but also the molecular structure of the binder, so that it is necessary to understand how the mechanical properties of a rubber depend upon molecular structure.

Finally, before proceeding with this study, it is appropriate to ask: what are the important modifications introduced by the filler? Experimental studies on propellants have shown three differences from unfilled rubbers. First, the tensile properties of filled rubbers are very different from their compression properties. Secondly, yield occurs in a series of steps; it may be necessary to distinguish among several types of yield. For example, it may be important, from the ballistic viewpoint, to define yield as the point at which the propellant has become porous enough, by virtue of mechanical strain, to increase its burning rate beyond a safe value. This critical porous strain may be less than the strain at which mechanical failure will occur. Thirdly, relaxation of stress progresses long after the rubber component has relaxed to its rubbery modulus; this indicates that a reshuffling of the adhesion bonds and positions of filler particles is a continuing process.

The next sections discuss the elastic fracture of rubbers and unfilled binders.

1. Unfilled elastomers

As the title of this section indicates, the materials with which we are dealing store energy reversibly until the time a crack appears. At this point, the energy released can in principle be accounted for by the kinetic energy and surface energy imparted to the new crack. The crack acts as a point of stress concentration but the local stress far away from the crack will remain below the yield stress of the material and thus continue to store energy elastically until the crack propagates through the material, at which time all the remaining strain energy will be recovered as kinetic energy.

Examples of such elastomers are natural rubber, butyl rubber, styrene-butadiene rubber (SBR, formerly GRS), polyurethane rubber, etc. All such rubbers evince large shear deformations prior to yield or cracking, and must therefore be characterized by a theory which allows for large deformations. Rivlin [10] has shown that the strain energy of a unit volume of undeformed rubber may be appropriately expressed as a function of three strain invariants, which, for an incompressible material, assume the form:

$$I_1 = \lambda_1^2 + \lambda_2^2 + \lambda_3^2 \tag{1-a}$$

$$I_2 = \frac{1}{\lambda_1^2} + \frac{1}{\lambda_2^2} + \frac{1}{\lambda_3^2} \tag{1-b}$$

$$I_3 = \lambda_1^2 \lambda_2^2 \lambda_3^2 = 1 \tag{1-c}$$

Where λ_i is the extension ratio of the coordinate acted on by the normal stress σ_i. Application of the principle of virtual work leads to the stress-strain relation* in terms of the true stress $\bar{\sigma}_i$:

$$\bar{\sigma}_i = \sigma_i \lambda_i = 2\left[\lambda_i^2 \frac{\partial W}{\partial I_1} - \frac{1}{\lambda_i^2}\frac{\partial W}{\partial I_2}\right] + \bar{k} \tag{2}$$

where $\bar{k}$ is, in general, a function of the coordinates, but not of the strain invariants.

In order to use (2), it is necessary to understand the nature of the strain energy density function W, and in particular, to procure an analytical representation which holds as close to rupture as possible. We shall take as our type material, for this study, unfilled natural gum rubber vulcanizate, the simple stress-strain curve for which is reproduced [11] in Figure 1. It is characteristic of natural rubbers that they possess a sharp increase in stress beyond 500% elongation. Most synthetic rubbers break near this elongation.

---

*When shear forces as well as normal forces are acting, the λ_i's are replaced by a set of appropriate strain tensors. In what follows, (2) will suffice.

An empirical method for rectifying simple tensile data[12] obtained on incompressible elastomers is based on the following observations. The initial portion of the stress-strain curve is fairly well represented by

$$\sigma = E\left(1 - \frac{1}{\lambda}\right) = E\,\frac{\lambda - 1}{\lambda} \tag{3}$$

which is equivalent to

$$\bar{\sigma} = E(\lambda - 1) \tag{4}$$

where $\bar{\sigma}$ is the true stress. Note that for large extension ratios (3) approaches the limiting value $\sigma = E$. In order to provide for the rapid increase in stress with later portions of the curve at large strain, (3) may be modified to

$$\sigma = E\,\frac{\lambda - 1}{\lambda^2}\,\lambda \quad \Rightarrow \quad \frac{E(\lambda - 1)}{\lambda^2}\, e^{\beta\left(\lambda - \frac{1}{\lambda}\right)} \tag{5}$$

which reduces to (3) for $\beta = \frac{1}{2}$ at small λ, i.e.,

$$e^{\frac{1}{2}\left(\lambda - \frac{1}{\lambda}\right)} \longrightarrow \lambda \tag{6}$$

One can use (5) by plotting (Figure 2)

$$\ln \frac{\sigma \lambda^2}{\lambda - 1} = \ln E + \beta\left(\lambda - \frac{1}{\lambda}\right) \tag{7}$$

where it is observed that the stress in kg/cm^2 is given by

$$\sigma = 7.39\,\frac{\lambda - 1}{\lambda^2}\, e^{0.416\left(\lambda - \frac{1}{\lambda}\right)} \qquad 1 < \lambda < 6 \tag{8-a}$$

$$\sigma = 0.705\,\frac{\lambda - 1}{\lambda^2}\, e^{0.80\left(\lambda - \frac{1}{\lambda}\right)} \qquad 6 < \lambda \tag{8-b}$$

We proceed to define $\lambda = 6$ as the yield point and observe that the modulus after yield is reduced by slightly more than a factor of 10, indicating that the network resistance has been drastically lowered. Since modulus is

proportional to cross links per unit volume, we infer that the loss in cross-link concentration arises from the slippage or tearing of entanglements, and that only the true chemical crosslinks remain to offer resistance. Support for this inference is deduced from the observation that the exponential factor now behaves more like λ^2 than λ, since β has doubled. This means that the load rather than the true stress is proportional to strain, the proportionality constant now behaving like a spring constant; lateral effects have suddenly become unimportant; the network loops now offer little or no resistance.

The exponential factor exp $\beta(\lambda-\lambda^{-1})$ is not amenable to quadrature and so the area under the curve in Figure 1 was evaluated stepwise by Simpson's Rule and the resulting strain energy plotted in Figure 3. This smooth monotonically increasing function of λ is nicely rectified by plotting W vs (I_1-3) as network theory [13] demands, (Figure 4). Again we note the yield at $\lambda = 6$. Prior to yield, the strain energy function is well represented by

$$W = \frac{\mu}{2}(I_1-3) \doteq 0.883\,(I_1-3) \qquad (9)$$

so that the shear and Young's moduli are approximately 1.76 kg/cm^2 and 5.28 kg/cm, respectively; this is a somewhat lower value than that obtained from Figure 2, but this is so because in (8) a higher E is needed to compensate for $\beta = \frac{1}{2}$; in other words, only the initial portion of the tensile curve can be represented in the form (8) with $\beta = \frac{1}{2}$ and E = 5.28.

The incompressibility of rubber all the way to rupture can be neatly demonstrated in the following way. In the case of simple tension, the strain transformation is given by

$$\lambda_1 = \lambda_2 = \frac{1}{\sqrt{\lambda}} \qquad (10)$$

$$I_1 = \lambda^2 + \frac{2}{\lambda} \quad , \quad I_2 = \frac{1}{\lambda^2} + 2\lambda \qquad (11)$$

The relations (10) and (11) hold only in the case of an incompressible material. Now assume that the strain energy function is given in the Mooney-Rivlin form

$$W = W_1(I_1 - 3) + W_2(I_2 - 3) \tag{12}$$

where W_1, W_2 are constants characteristic of the material; we have chosen $W_1 = .883$, $W_2 = 0$. The slope of the curve in Figure 4 is given by

$$\frac{dW}{dI_1} = W_1 + W_2\frac{dI_2}{dI_1} = W_1 + \frac{1}{\lambda}W_2 \doteq W_1 \tag{13}$$

in our case; similarly

$$\frac{dW}{dI_2} = W_2 + \lambda W_1 \doteq \lambda \frac{dW}{dI_1} \tag{14}$$

Figure 5 shows a plot of W vs. (I_2-3); it is easily verified that the slope at any point, dW/dI_2, is exactly equal to λ times the slope dW/dI_1 of Figure 4 right out to rupture. Thus the discontinuities observed in Figures 2 and 3 are not to be associated with density changes.

We turn now from a description of the material characteristics of unfilled elastomers to those of the filled material.

2. Filled elastomers

The most striking difference between filled and unfilled elastomers is the so-called blanching phenomenon or pullaway of the binder from the filler. As indicated in the introduction, this makes for three observations. First, the pullaway occurs in steps, undoubtedly depending upon the distribution of adhesion bond strengths between oxidizer and binder. Second, it does not occur in compression. Third, after pullaway, relaxation not of the network, but of the strain energy located at the surface of the void spaces, occurs. This is demonstrated by the fact that a filled rubber, after three months at constant strain (30%), will relax its modulus from 500 psi

to 5 psi. And then, upon complete recovery of the applied strain at the end of a second three months, will resume its initial modulus minus the contribution that arose from the adhesion to the filler. If this cycle be repeated a second time, the modulus will relax and return to roughly the same values.

Because of this reversible shuffling back and forth of the filler particles, it follows that the time rate of change of the local stress distribution in a filled rubber must be quite complicated and that the rupture criterion may be significantly more complex than that which is proposed above for an unfilled rubber. One can start by neglecting relaxation, ie., working with short time data. On this basis then, the curvature of a tensile curve is to be ascribed entirely to pullaway effects without reshuffling. The modulus decreases because adhesion bonds are broken and because the propellant dilates. This dilation effect is shown in Figure 6 where Poisson's ratio is plotted vs. axial strain, the strains having been carefully measured photographically. Figure 7 shows how the modulus is increased in the region of negative strain or compression. The question arises: what sort of elastic behavior is evinced by such a material when it is subjected to combined tension and compression?

A relatively simple case arises in the pressurization of an infinitely long hollow unbonded tube of propellant, internally pressurized, the analysis of which will be pursued here. Since the algebra is quite involved, only the essential features will be sketched. It is thought that this type of analysis will become increasingly important as the nature of the pullaway effect becomes more completely understood.

As a result of internal pressurization, all radial and axial elements of the propellant tube are in compression. The hoop elements, however, are in tension so that an orthotropic response may occur. Jaeger[14] shows that for such a case, where the orthotropic material properties are with respect to cylindrical coordinates, the stress-strain relations are

$$\sigma_\theta = C_{33}\epsilon_\theta + C_{13}\epsilon_r + C_{13}\epsilon_z \qquad \tau_{r\theta} = C_{44}\gamma_{r\theta} \qquad (15)$$

$$\sigma_r = C_{13}\epsilon_\theta + C_{11}\epsilon_r + (C_{11}-2C_{66})\epsilon_z \qquad \tau_{\theta z} = C_{44}\gamma_{\theta z}$$

$$\sigma_z = C_{13}\epsilon_\theta + (C_{11}-2C_{66})\epsilon_r + C_{11}\epsilon_z \qquad \tau_{rz} = C_{66}\gamma_{rz}$$

By analogy with isotropic theory, we have

$$\begin{aligned} C_{66} &= \mu \\ C_{33} &= \lambda_{TT} + 2\mu \\ C_{13} &= \lambda_{TC} \\ C_{11} &= \lambda_{CC} + 2\mu \end{aligned} \tag{16}$$

Since the hoop direction is the only one in tension, C_{33} is the coefficient that one would measure in triaxial tension, of the type described in Section II, so that $(C_{33}-2\mu)$ is indicated by the Lamé constant with a double subscript T. Likewise, $(C_{11}-2\mu)$ is the Lamé constant one gets from triaxial compression, and is designated by the double subscript C. The coefficient C_{13} is an interaction coefficient which could be measured in mixed triaxial compression tension, i.e., pulling in one direction and squeezing on the two sides. In pure compression, the constants become

$$C_{33} - 2\mu = C_{13} = C_{11} - 2\mu = \lambda = K - \tfrac{2}{3}\mu \tag{17}$$

where K is now the hydrostatic bulk modulus in compression. In the problem at hand, we have

$$\sigma_\theta = C_{33}\frac{u}{r} + C_{13}\frac{du}{dr} \tag{18-a}$$

$$\sigma_r = C_{13}\frac{u}{r} + C_{11}\frac{du}{dr} \tag{18-b}$$

$$\sigma_z = C_{13}\frac{u}{r} + (C_{11}-2\mu)\frac{du}{dr} \tag{18-c}$$

where u is the radial displacement. Substitution of (18) into the equation of stress equilibrium

$$\frac{d\sigma_r}{dr} + \frac{\sigma_r - \sigma_\theta}{r} = 0 \tag{19}$$

yields

$$\frac{d^2u}{dr^2} + \frac{1}{r}\frac{du}{dr} - \frac{C_{33}}{C_{11}}\frac{u}{r^2} = 0 \tag{20}$$

Note that, by direct observation, $\lambda_{rr} \ll \lambda_{cc}$ (because of the pullaway effect) and therefore $C_{33}/C_{11} < 1$. The solution of (20) is given by

$$u = A r^{k} + B r^{-k} \tag{21}$$

$$\sigma_r = \frac{A}{r^{1-k}}\left(C_{13} + \sqrt{C_{11}C_{33}}\right) + \frac{B}{r^{1+k}}\left(C_{13} - \sqrt{C_{11}C_{33}}\right) \tag{22}$$

where $k = (C_{33}/C_{11})^{\frac{1}{2}}$. The constants A and B can now be evaluated at r = a, and r = b, where $\sigma_r = -P$ and 0 respectively. The result is

$$\frac{\sigma_r}{P} = -\frac{\left(\frac{b}{r}\right)^{1+k} - \left(\frac{b}{r}\right)^{1-k}}{\left(\frac{b}{a}\right)^{1+k} - \left(\frac{b}{a}\right)^{1-k}} \tag{23}$$

$$\frac{\sigma_\theta}{P} = k\,\frac{\left(\frac{b}{r}\right)^{1+k} + \left(\frac{b}{r}\right)^{1-k}}{\left(\frac{b}{a}\right)^{1+k} - \left(\frac{b}{a}\right)^{1-k}} \tag{24}$$

$$\frac{1}{P}\frac{u}{r} = \frac{k\left[\left(\frac{b}{r}\right)^{1+k} + \left(\frac{b}{r}\right)^{1-k}\right] + \frac{C_{13}}{C_{11}}\left[\left(\frac{b}{r}\right)^{1+k} - \left(\frac{b}{r}\right)^{1-k}\right]}{C_{11}\left[k^2 - \left(\frac{C_{13}}{C_{11}}\right)^2\right]\left[\left(\frac{b}{a}\right)^{1+k} - \left(\frac{b}{a}\right)^{1-k}\right]} \tag{25}$$

Note that if $C_{13}/C_{11} > k$, the radial displacement is negative. However this is not physically possible since the work done by the internal pressure must always be positive; hence one should find experimentally that $C_{13}/C_{11} \leq k$. Further, when $C_{13}/C_{11} = k$, there is no singularity as can be seen by taking limits carefully. The most significant difference from the isotropic case arises in the occurrence of fractional rather than integral exponent powers of the radial coordinate.

This same treatment can be applied to the case-bonded propellant. It will be necessary in this and many other situations to solve for the point at which the hoop stress changes sign. By following this procedure, one can avoid trial and error techniques. In general, problems of this nature will best be solved with the aid of digital computational aids. Before programming, however, it will be necessary to determine the strain energy function for the propellant in both compression and tension. The theory of finite elastic deformation of anisotropic materials has been presented by Rivlin and Erickson[15] so that, in principle, the pullaway effect can be handled all the way to rupture if the strain energy density function is known.

C. Uniaxial Test Data

Considering the implied necessity for obtaining material property data for fracture investigations, such as the strain energy density function just mentioned, it is appropriate to review some of the current tests commonly being conducted, and their applicability to the problem at hand.

1. Standard variable strain rate testing

By far the largest accumulation of data relates to fracture under simple uniaxial tension. For solid propellant materials these tests have normally been conducted on standard JANAF specimens (Figure 8) at variable strain rates and temperatures. One common testing machine is the Instron tester which will impose constant crosshead motion through a range of speeds from 0.02 to 20 inches per minute, over a temperature range between $-100^{\circ}F$ and $160^{\circ}F$. The output of the machine is an automatically recorded force-time trace to fracture (Figure 9) which provides the basic experimental information. Depending upon the magnitude of strain to fracture, the data is converted into plots of nominal or true stress, i.e. force divided by original or actual cross sectional area, versus strain. The accuracy of the latter quantity is frequently open to question because the elongation, or crosshead separation, is not distributed evenly over the specimen length and some "effective length" must be selected. It is common practice to use an effective length of 2.7 inches for the JANAF specimen.

This uncertainty in the basic data emphasizes the desirability, and near necessity, of developing local strain indicating devices for low modulus materials. Several improvements along these lines have been attempted, such as using gage marks near the center of longer specimens, or circle patterns distributed over the length. While some increase in accuracy has been reported, the data serve also to indicate in many cases a basic nonhomogeneity in strain distribution due to the filler particles in the propellant.

Neglecting nevertheless these important experimental refinements and working only with the reduced experimental stress-strain data, one turns next to the problem of organizing the extensive test information for many temperatures and strain rates in useful form. Presuming for the most part that maximum stress, σ_m, and strain at maximum stress, ε_m, are the significant quantities (the slope of the curve, or modulus, is also used in model representation) Smith has shown for a wide variety of polymers that a

very reasonable correlation of ultimate tensile properties can be obtained if the data are plotted against the logarithm of a reduced time parameter, $a_T R$, where R is the constant strain rate at which the test was conducted and a_T is the Williams, Landel, Ferry (WLF) temperature shift factor,

$$\log a_T = \log \frac{t}{t_R} = \frac{c_1 (T - T_S)}{c_2 + T - T_S} \qquad (26)$$

a_T can also be interpreted as the ratio of the time to measure some phenomena at temperature T to the time to measure the same phenomena at the reference temperature T_S.

A set of typical strain data is shown in Figure 10, and similar stress data in Figure 11. Note in the latter case the stress has been normalized by a temperature ratio because polymer theory predicts a linear increase of retractive forces with absolute temperature. Both sets of data were normalized by using the temperature shift factor, experimentally deduced from separately shifting (i) strain at ultimate stress data, (ii) maximum stress data, and (iii) modulus data, and finding all three agreed if $c_1 = -8.86$, $c_2 = 101.6$ and $T_S = 269^\circ K$. That such a convenient and near universal correlation exists for ultimate properties is extremely useful, and among other things, permits one to predict with fair precision the uniaxial tensile fracture behavior over wide ranges of strain rate and temperature from a limited set of test data.

Before passing on to a consideration of fracture under multi-axial load conditions, it should be observed that the temperature shift correlation is reasonably well founded experimentally but that the limited strain rate capability of the Instron tester is not particularly well suited for verifying the correlation over wide extremes. This may be noted in Figure 10 where the test data at various temperatures barely overlap. One would feel much more confident if, for example, the open circle ($160^\circ F$) data obtained over the $1/R a_T$ range 5 to 8 could be extended to lower values by increasing the strain rate, hence lower $1/R\, a_T$, at the same $160^\circ F$ temperature. Bearing in mind however the limitation of the tester, approximately 20 inches per minute crosshead motion maximum, it is impossible to fulfill this desire without changing the specimen, which would not be particularly acceptable.

2. High strain rate testing

The obvious answer is to inquire if higher rate testers would be available. Several have been developed. One of these is the Allegheny Instrument Company device[17] which is generally well known. Another is one developed by E. I. Du Pont de Nemours and described in a recent paper by Jones[18]. Basically this latter machine, which achieves high loading rates by means of a controlled explosion of smokeless powder in the head, can strain JANAF specimens up to approximately 200,000 inches per minute. While it is premature to generalize, indications from this and other high speed tester work are that the theoretical W LF shift factor for ultimate fracture of tensile JANAF specimens is valid for engineering purposes.

D. Multiaxial Testing

Inasmuch as the uniaxial testing procedures for simple JANAF tension specimens are well known and data reduction techniques widely disseminated, the subject has been rather shortly dismissed. On the other hand, from a structural standpoint as distinguished from the quality control objective, the important subject of the fracture behavior of viscoelastic materials subjected to biaxial and triaxial loadings needs considerable amplification, but suffers from lack of experimental data. At the present time, it is proposed to discuss some possible experiments in this area with particular emphasis upon their suitability for solid propellant materials and due regard for testing equipment convenience.

1. Pressurized tensile tests

Perhaps one of the simplest extensions of the present uniaxial tensile test using the Instron tester is to enclose the specimen in a leak proof container filled with air or liquid maintained at an arbitrary compressive pressure. Within the same criticisms of the basic test with no external pressure, a triaxial tension-compression stress field can be imposed. Suppose that the geometry is as shown on the sketch. Then the stress and strain analysis for the central portion of the specimen subjected to the uniaxial tensile stress gives

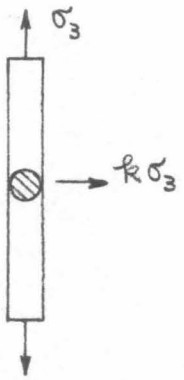

$$\sigma_3 = \sigma \; ; \quad \varepsilon_3 = \frac{\sigma_3}{E}\left[1 - 2\nu k\right] \tag{27}$$

$$\sigma_1 = \sigma_2 = k\sigma \; ; \quad \varepsilon_1 = \varepsilon_2 = \frac{\sigma_3}{E}\left[-\nu + (1-\nu)k\right] \tag{28}$$

One would expect therefore an apparent uniaxial modulus for this triaxial field of

$$E_a = \frac{E}{1-2\nu k} \tag{29}$$

where, because in the tests as described k is negative corresponding to a compressive stress, the apparent modulus would be smaller than the uniaxial modulus. For small strains it would in principle be possible to deduce the (elastic) value of Poisson's ratio.

As in the former case, these tests could be conducted at various strain rates and temperatures.

2. Poker chip tests

Another test that may be conducted with relative ease consists of cementing a thin circular disk of propellant between two parallel end faces of two circular steel plates being subjected to tension. The softer disk sandwiched between the harder bars will be restrained, because of its thinness, from its usual contraction perpendicular to the load and hence generate a triaxial tension stress field.

The elementary analysis for this case may be made by assuming the disk infinitely thin such that the external radius is sufficiently far from the center to assume the only non-zero displacement, w, is in the axial direction. Under these conditions, one is led to deduce for small deformations

$$\sigma_3 = \sigma \; , \quad \varepsilon_3 = \frac{\sigma(1-2\nu)(1+\nu)}{E(1-\nu)} \tag{30-a}$$

$$\sigma_1 = \sigma_2 = \frac{\nu}{1-\nu}\sigma \; ; \quad \varepsilon_1 = \varepsilon_2 = 0 \tag{30-b}$$

so that the apparent axial modulus becomes

$$E_a = E\left[\frac{1-\nu}{(1-2\nu)(1+\nu)}\right] \tag{31}$$

where it may be noted that for propellants, which are characteristically nearly incompressible, i.e., $\nu = \frac{1}{2}$, the triaxial tension approaches hydrostatic with a consequent infinite apparent axial stiffness.

A fairly extensive and revealing investigation into the use of this test for an incompressible rubber has been reported in two papers by Gent and Lindley [19-20]. When one attempts to improve the analysis outlined above, the major difficulty arises in determining the stresses and strains throughout the disk. Whereas the previous analysis assumes the edges are infinitely far from the center, in the actual test piece there will will be a local necking of the propellant, however slight, as the assembly is subjected to tension. When this effect is accounted for the analysis becomes considerably more complicated. For an incompressible material, Gent and Lindley have given an approximation to the apparent axial modulus which depends on the thickness, h, of the disk of radius a,

$$E_a = E\left[1 + \frac{1}{2}\left(\frac{a}{h}\right)^2\right] \qquad (32)$$

where it may be observed that the apparent modulus, as before, becomes infinite as the thickness approaches zero.

Furthermore their fracture data, reproduced in Figure 12, shows for the various compositions indicated by the different curves that the axial stress to cause fracture increases as the disk thickness decreases. They have suggested that the limit for zero thickness is twice the value for large thickness. While it is tempting to thus extrapolate the data, it is not unreasonable to expect the curve near zero h/a to change slope. Realizing that the breaking stress used by Gent and Lindley is in reality an averaged stress over the face of disk, it would be appropriate to obtain an improved approximation. This can actually be obtained using the principle of minimum complementary energy. The outline of such a solution given in Appendix 5.1, and not restricted to incompressible materials, predicts a stress distribution that is a power law in the radius and hyperbolic in the thickness, and for the limiting situation of zero thickness (infinite radius) gives the proper limiting value $\sigma_r / \sigma_z = \nu/(1-\nu)$. Further remarks upon the utility of this solution in interpreting the experimental failure data will be reserved until later.

By conducting such tests as reported above, using an Instron tester, the usual ranges of interest in strain rate and temperature can be covered and the possibility of strain rate, temperature shift explored.

3. Torsion of rod specimens

Among the various types of mechanical testing, torsion stands as particularly important. There are several reasons for this. First of all, a cylindrical specimen subjected to a small angle of twist undergoes pure shear; the applied torque is directly proportional to the measured twist angle per unit length, the proportionality constant being the shear modulus. Thus the torsion properties for small strain should be independent of Poisson's ratio.

As the shear strain is increased, however, new effects enter the picture. Finite elastic theory predicts a lengthening of the specimen known as the Poynting effect.

It may be deduced that

$$\lambda^3 = 1 + \frac{k^2}{4}\left(b^2 - a^2\right) \tag{33}$$

where λ is the axial extension ratio

a, b are the inner, outer radius of the cylinder respectively

k is the angle of twist per unit length

One obtains (33) by application of finite elastic theory to the strain transformation defined by

$$\bar{r} = \frac{r}{\sqrt{\lambda}}$$

$$\bar{\theta} = \theta + kz$$

$$\bar{z} = \lambda z$$

The undetermined constant which enters into the theory because of the incompressibility condition is determined by setting the integral of the axial stress over the end face equal to zero. Figure 13 shows a plot of $\lambda^3 - 1$ vs k^2, taken from recent data[21] on polyurethane propellant. Note

the excellent straight line correlation in agreement with theory. The theoretical value of the slope is 1/8 in^2/ rad^2, whereas the measured value turns out to be 1/7 in^2/ rad^2. Considering the assumptions made in deriving (33), the agreement is excellent. The most important observation that can be deduced from this is that the elastic properties of the binder predominate at least up to 3% shear strain. A similar type of verification is provided by the recent data of Bergen, Messersmith and Rivlin on filled rubbers[22].

On the other hand, indications are the elongation will decrease as the twist is increased further. This is to be expected since the pullaway of the binder from the filler will tend to convert the local shear into local simple tension around the filler particles. What effect this will have upon fracture in torsion is not known. It is suspected that the fracture criterion will not be as simple for a filled elastomer as an unfilled one, therefore torsion should provide an excellent way to check out the applicability of the distortion strain energy criterion. Furthermore, torsion under superimposed hydrostatic pressure can then be used to check out the importance of anisotropy.

4. Hollow tube tests

Providing a satisfactory strain measurement is available, the behavior of an internally pressurized thin or thick walled cylinder up to and including burst would yield fracture information under biaxial tension, for zero axial stress, or with the added triaxiality depending upon the nature of a finite longitudinal stress. This type of specimen has been used with mixed success at the U.S. Naval Ordnance Test Station[23] employing an oil for the pressurization. The major difficulties aside from such obvious ones as preventing leakage, are to obtain an accurate strain history and to measure the applied time varying pressure. These tests can be used upon either thin or thick walled cylinders, and with or without being enclosed in a case. In some cases it will be more convenient to check out a thin case-bonded design using externally mounted wire strain gages and inferring the tube, or even star point, strains by working backward using the theoretical solution. For most purposes however, the resultant case to grain stiffness is so high that accuracy is poor.

The main advantage of such a test is its reasonably close similarity to an actual operational configuration. If the pressure-time rise is appropriately regulated, the test could be useful in predicting fracture under a varying and typical strain rate history.

It should also be mentioned that it is possible to extend the rod torsion tests mentioned in the preceding section to hollow cylinders, preferably thin walled because of the relative accuracy with which the theoretical solution is known. Shank [24] has recently undertaken some exploratory work in this area although it is expected some time will elapse before definitive results are obtained. Another test variation using the hollow tube is the possibility of using this geometry to examine the effect of orthotropy of multi-layered cylinders. Some preliminary analysis along these lines was presented by Pister in the third progress report. Some unpublished results of his continuing program, including some planned experiments, should furnish evidence for or against the desirability of this test geometry for orthotropic propellant media studies.

5. Crack propagation tests

Multiaxial testing can also be extended to include the biaxial stress field which exists near the point of a crack in a medium which has already begun to fracture. We consider several initially cracked configurations and their associated stress fields.

a. Thin sheets subjected to stretching:- A common configuration for metal sheet specimens not used extensively for propellants is the tensile strip containing a crack perpendicular to the load. This test is used to determine critical crack length, i.e., to find what size crack or flaw a given material of specified thickness will sustain under a specified external stress before it becomes unstable and propagates catastrophically.

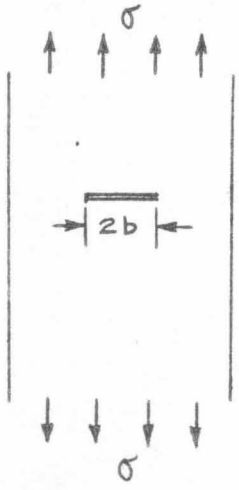

A considerable amount of test data and test technique has been accumulated, particularly in the aeronautical field. The test results are usually presented as in Figure 14. The main distinction between metals and propellants, of course, is the sensitive strain rate dependency of the latter. One suspects that a stressed specimen with a critical crack will not "let go" but rather begin to fracture, at higher than impact rates, in more of a tearing fashion.

A series of exploratory tests was conducted by McCullough [25] upon specimens one-quarterinch thick and two inches wide containing an initial crack two-tenths of an inch long. For experimental convenience, these were conducted at essentially constant strain and held until the crack began to grow and the stress simultaneously relaxed. Typical data is shown in Figure 15.

A somewhat general elastic analysis for this geometry has been presented by Ang and Williams[26] for an orthotropic sheet subjected to combined stretching and bending, assumed infinitely wide with respect to the initial crack length 2b. This elastic solution as might be expected suffers from the fact that it predicts infinite stresses at the crack tip which are of course physically inadmissible. On the other hand one can hypothesize the the existence of a region of constant finite stress with a characteristic radial extent which would give a stress distribution such as shown in the sketch.

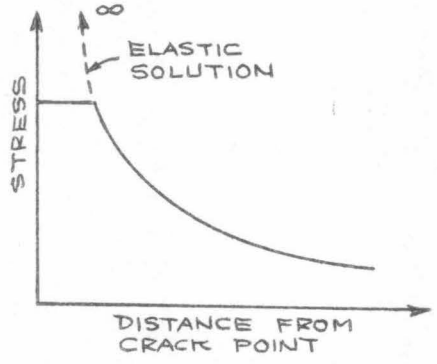

For problems where the boundary conditions are prescribed solely upon the stress, it will be recalled that the viscoelastic analogy permits one to conclude that the viscoelastic stress distribution is identical with the elastic one. This experimental specimen geometry is a case in point if the "plastic" region is neglected because all boundaries, including the crack, are stress free except at the loading jaws where it may be assumed the (uniform) stresses are prescribed. Hence one may, for example, use the Ang-Williams elastic solution, reduced to the case of stretching in an assumed isotropic sheet to give the viscoelastic stresses, along the line of crack propagation for example, as

$$\sigma_x(x,0) = \frac{\sigma_0 b^2}{\sqrt{x^2-b^2}\,[x+\sqrt{x^2-b^2}]} \quad ; \quad x>b$$

$$= \sigma_0\left\{1/\sqrt{\frac{2\epsilon}{b}} - 1 + O\left[\left(\frac{\epsilon}{b}\right)^{\frac{1}{2}}\right]+\cdots\right\} \quad ; \quad x=b+\epsilon \qquad (34)$$

$$\sigma_y(x,0) = \sigma_0\left\{1+\frac{b^2}{\sqrt{x^2-b^2}\,[x+\sqrt{x^2-b^2}]}\right\} \quad ; \quad x>b \qquad (35)$$

$$= \sigma_0\left\{1/\sqrt{2\epsilon/b} + O\left[\left(\frac{\epsilon}{b}\right)^{\frac{1}{2}}\right]+\cdots\right\} \quad ; \quad x=b+\epsilon$$

It may be noted that at the crack point the solution predicts a two-dimensional hydrostatic tension described in detail elsewhere[27].

The viscoelastic strains and deformations are obtained in the usual fashion. It is necessary only to insert the Laplace transform of the pressure-time loading into the solution for stresses above, integrate for the displacements, and complete the inverse transform for the physical displacements.

From the fracture standpoint, however, the analysis is only partially completed. As stressed in the introduction, the strain analysis due to a given loading must be supplemented by predicting the load for which fracture will occur, or in this case, for which the crack will begin to grow. An analysis has been presented in Appendix 5.2 giving the velocity of crack propagation as a function of the allowable one-dimensional strain ε^* and the radius of the enclave, δ, over which it is presumed constant. The simple analysis for a constant applied stress, σ_0, has been carried out using a two element viscoelastic model and leads to the result that the velocity of the crack point, v_n, at a distance $n\delta$ from the original position is

$$v_n \approx \frac{\pi}{2\sqrt{2}}\,\frac{\sigma_0/E_v}{\epsilon^*}\,\frac{b}{2}\sqrt{\frac{n\delta}{b}\left(1+\frac{n\delta}{b}\right)} \qquad n \geq 4 \qquad (36)$$

In principle, therefore, it would be possible to carry out the calculations for the constant strain loading used by McCullough and deduce the appropriate value of δ, if it exists. On the other hand, and considering the exploratory nature of his early tests, a newset is being conducted based upon a constant applied stress for which the foregoing analysis is directly applicable. It should be emphasized however that δ, estimated in Appendix 5.2 to be of the order of one thousandth of an inch, is still an experimental parameter to be determined, although physically it may be thought of as the effective diameter of a strand or bundle of polymer chains which act together.

b. Thin sheets subjected to bending:- Another configuration of considerable interest is an initially cracked specimen subjected to bending. One common form is the peel or tear test, but, instead of testing adhesive strength to another material such as a propellant case, suppose a cantilever sheet specimen was bent as indicated in the sketch. It can be shown that there is a biaxial stress at the base of the tear and one could attempt to analyze the resulting stresses and strains. Alternately one could consider, for example a long cylindrical tube with a wedge cut out where the wedge approaches zero so that one would have a plane fracture surface (see sketch). This situation would correspond somewhat to a crack along a star valley where the wedge angle was adjusted appropriately. Finally one could subject the same cracked geometry as used in the tensile loading situation to bending. Generally speaking, however, grains are not customarily loaded as indicated in the first and third sketches, and thus these bending configurations are not of such immediate use except insofar as they assist in interpreting the mechanics of fracture. Explicit solutions for the first situation are not presently available but the Ang-Williams solution can be applied to the strip containing a crack. The "log-splitting problem" however has been considered theoretically[28, 29, 30] and gives some estimates of the biaxial distribution. At the present time, however, they do not appear quite as ready for interpreting possible tests as other suggestions previously made.

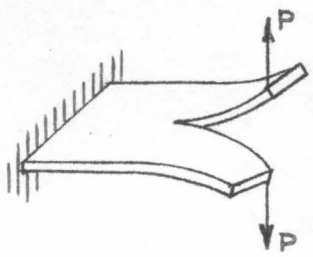

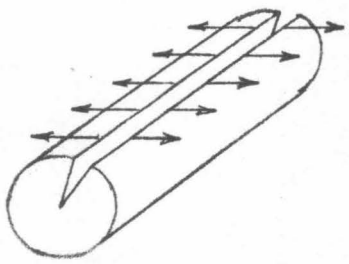

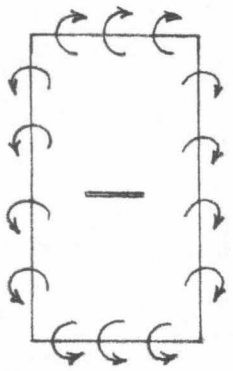

c. Pressurized membrane:- One final test to be described concerns a circular sheet of propellant mounted over the top of a gas or liquid pressure source - much like a drum head subjected to internal pressure. The stress distribution at the center is uniform tensile - tensile and determinable if the bending is considered a small effect. Further the volume change can be measured, or strain indicators mounted on the specimen to give stress-strain behavior under equal tension. It is also possible to insert central or radial cracks in the specimen along with suitable sealing, and prepare curves of critical crack length as a function of applied pressure. It is suggested, however, that it may be of more immediate value to explore the results of some of the tests more readily adapted to current equipment, and exploit the resulting data first, before considering the types of tests outlined in (b) and (c).

E. Selection of the Failure Criterion

It is practically impossible to select a failure criterion without fairly complete experimental data, although some interesting comparisons can be drawn among the available criteria. In order to illustrate the type of correlation being sought and how it might be treated, we shall discuss three criteria thought to be among the more likely candidates.

1. Illustrative fracture criteria

The criteria considered are maximum distortion energy based upon stress, maximum distortion energy based upon strain, and maximum normal strain.

a. Stress distortion: - In this case one assumes that the sum of the squares of principal stress differences, which is proportional to the stress producing a distortion as opposed to dilatation, is constant. Furthermore, the constant σ_{uni} is determined from the uniaxial stress at fracture* so that

$$\sigma_{uni} = \left(1/\sqrt{2}\right)\sqrt{(\sigma_1 - \sigma_2)^2 + (\sigma_2 - \sigma_3)^2 + (\sigma_3 - \sigma_1)^2} \qquad (37)$$

Note that for the uniaxial tensile specimen, $\sigma_1 = \sigma_2 = 0$, and $\sigma_3 = \sigma_{uni}$ as expected.

Consider now the same specimen, but in addition let it be subjected to a lateral pressure stress (D, 1 above) such that $\sigma_1 = \sigma_2 = k\sigma_3$. (These latter stresses are equal from consideration of the equations of equilibrium.) The allowable stress is then found upon substitution into the criterion to be:

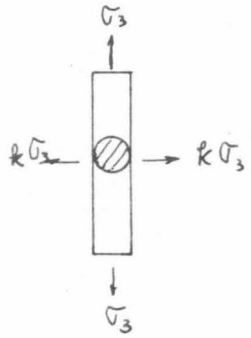

$$\frac{\sigma_3}{\sigma_{uni}} = \frac{1}{|1 - k|} \qquad (38)$$

* Actually the stress at yield, in usual applications, where the onset of yielding is defined as failure.

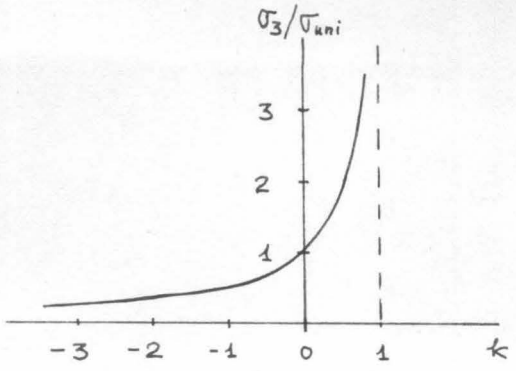

which variation is shown in the sketch. It shows that a lower than purely one dimensional allowable stress would be expected if the side stress was compressive, whereas a higher value is anticipated for tension. Note that no limit stress is predicted if the stress distribution approaches hydrostatic tension.

Test results for a pressurized specimen would thus be plotted on the predicted curve, with correlation tending to substantiate the stress distortion criteria.

b. Strain distortion: - If now, on the other hand, one were to postulate that distortion shearing strain was to trigger failure, then the criterion in terms of principal strain would be

$$\epsilon_{uni} = \frac{1}{(1+\nu)\sqrt{2}} \sqrt{(\epsilon_1 - \epsilon_2)^2 + (\epsilon_2 - \epsilon_3)^2 + (\epsilon_3 - \epsilon_1)^2} \qquad (39)$$

Upon taking account of symmetry in the stress-strain relations such that $\epsilon_1 = \epsilon_2$, one has for the same loading condition on a pressurized specimen as in a, above

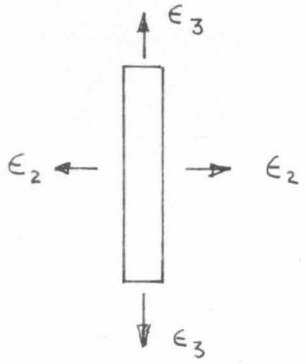

$$\epsilon_1 = \epsilon_2 = \frac{\sigma_3}{E}\left[-\nu + (1-\nu)k\right] \qquad (40)$$

$$\epsilon_3 = \frac{\sigma_3}{E}\left[1 - 2\nu k\right] \qquad (41)$$

Thus, substitution into the criterion yields for the allowable strain compared to that in the purely uniaxial stress condition

$$\frac{\epsilon_3}{\epsilon_{uni}} = \frac{1 - 2\nu k}{1 - k} \quad ; \qquad \epsilon_{uni} = \frac{\sigma_{uni}}{E}\left[1 - 2\nu k\right] \qquad (42)$$

which is easily checked by taking $k = 0$. For the more general triaxial stress condition, however, the criterion becomes dependent upon not only

the amount of triaxiality k , but also Poisson's ratio, ν . This variation is shown in the sketch. Perhaps the most interesting observation which can be made is that for Poisson's ratio of one half, typical of incompressible materials, the predicted maximum allowable strain due to triaxial stress is identical to the maximum (uniaxial) strain. Hence, if substantiated by test data, one would expect that whenever the strain at a point in an incompressible media exceeds the one dimensional value - which is actually the maximum principal strain criterion - failure would be predicted. Note also that while precisely true for $\nu = 1/2$, for $\nu \to 1/2$ the coïncidence is quite close over a large range of stress ratios.

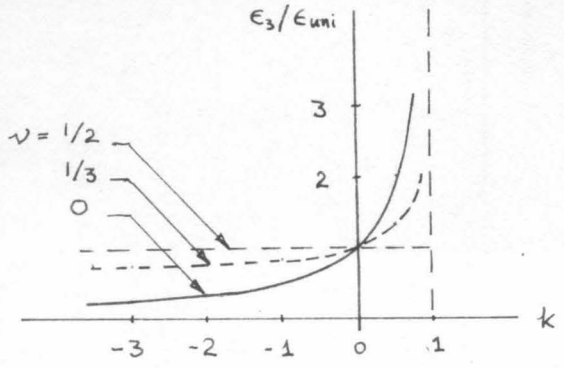

Note finally that no limiting strain is predicted if the strain distribution becomes hydrostatic tension.

c. Maximum normal strain: - A criterion based upon this premise is one of the simplest to use because it requires only a knowledge of how much (principal) strain can be imposed, as determined by a uniaxial stress test. Furthermore, in the particular case of a combined field, it corresponds for an incompressible body to the distortion strain limit. As in any of the criteria, however, test data is required in order to establish the validity of any particular postulate.

2. Various combined stress fields

The selection of a criterion is difficult because, if universally applicable, it must work for any combination of stresses. In the general situation, there are three principal stresses, each of which may be either tensile or compressive. A convenient way of representing the combined stress is to plot the stresses at a point in terms of rectilinear coordinates (σ_1 , σ_2, σ_3). Thus any state of stress will fall in one of the eight octants. Normally, however, any single experiment will only check out one or two of the octants, and thus several tests or types of tests must be carried out to test the hypothesis in tension-tension-tension , tension-compression-compression, etc.

With propellant materials, and especially filled propellants, there is an additional complication because of the potentially different behavior of the material itself in tension and compression associated with pull-away of the filler from the elastomer.

Notwithstanding the difficulty in the experiment or analysis, it is considered expedient to establish as many fracture limits as possible in the various octants to permit the establishment of a temporary working hypothesis, crude as it may be. We consider first the case of unfilled elastomers.

3. Unfilled elastomers

a. Possible criteria for fracture: - Most materials evince three distinct regions of mechanical interest. There is an initial region of elastic behavior in which energy is stored up reversibly. In the case of a metal, this behavior extends only over a few tenths of a per cent of strain, which strain is recovered completely without hysteresis, and the associated stress is linearly related. In the case of a cured rubber, the elastic behavior extends out to several hundred per cent strain, which is recovered completely without hysteresis;the associated stress, however, is related in a non-linear fashion as indicated by eqn. (28). In the case of a plastic, the elastic range may barely exist. When it does, as in the case of polymethyl methaerylate, it extends only over a few per cent, and may or may not be linear over the whole range.

The hysteresis phenomenon arises from internal frictional processes and gives rise to the study[31] of viscoelasticity*. Most viscoelastic materials are linear in their flow properties and obey the principle of temperature-time equivalence as discussed earlier[16]. This makes for convenience in superimposing data obtained at various temperatures. The distribution function which characterizes the friction processes embraces a large range of materials from unfilled rubbers to plastics (see the fifth progress report), so that it is common parlance to talk of reduced equations of state for polymeric materials in general.

---

* The term viscoelastic, as used here, is distinguished from plasticity by being restricted only to materials which recover completely, or almost completely.

When a filler is introduced into an elastic material, new types of friction processes are introduced. Thus, cured rubber which is essentially non-viscoelastic at room temperature becomes highly so when filled. The rate and frequency dependence of the associated relaxation in a highly filled rubber does not appear to be linear, nor does it appear to obey the temperature-time equivalence principle. For this reason, special techniques are needed for analyzing data on filled rubbers in the elastic region. A further discussion of this will be presented at a later time.

As the strain is increased, most materials at some point begin to show marked deviation from elastic behavior. If the substance is a metal, it may suddenly undergo plastic flow in which case the yield point is clearly marked. A rubber or propellant on the other hand will start to tear with no marked yield point. A plastic will in some cases undergo plastic flow and in other cases fracture in a brittle fashion, depending upon the rate of strain.

After yield, local stress conditions predominate in most materials. Depending upon the state of purity or the method of sample preparation, a given specimen will contain a number of defective or weak sites which will act as loci of stress concentration. For polymeric materials, it is generally true that the more brittle the material, the less sensitive to defects is the ultimate or fracture stress, as in the case of a plastic or rubber below its transition temperature. In the case of a highly filled rubber tested at room temperature, large batch-to-batch variations in tensile strength are observed despite careful efforts to control the formulation. Thus, in dealing with such materials, it is better not to use the fracture point but rather the yield point for design purposes, which of course has the further advantage of being conservative.

As enumerated earlier, various criteria have been proposed to define the point at which yield or fracture will occur. In addition, it should be noted that for large strains it is necessary to distinguish between the mean deviatoric stress(37) and the distortion strain energy(9). In particular, the maximum strain difference is defined as the difference of the finite strain $(1/2)(\lambda_i^2 - \lambda_j^2)$. The mean deviatoric stress is obtained by substituting (2)and (9) into the expression

$$\bar{\sigma}_d = (1/\sqrt{2})\sqrt{(\bar{\sigma}_i - \bar{\sigma}_j)^2 + (\bar{\sigma}_j - \bar{\sigma}_k)^2 + (\bar{\sigma}_k - \bar{\sigma}_i)^2} \qquad (43)$$

$$= \mu\sqrt{I_1^2 - 3I_2}$$

Note that this expression, after squaring, does not yield the distortion strain energy proportional to I_1-3 as is accomplished in infinitesimal theory. Thus a new criterion develops for elastomers. Lastly, the total strain energy is identical to the distortion strain energy for an incompressible material. No further allusion will be made to total strain energy until dealing with filled elastomers. It is instructive to tabulate these criteria for an incompressible material subjected to both uniaxial and biaxial tension. Since we are dealing with elastomeric materials, finite elastic deformations must be accounted for. In Table I, the ultimate value of the uniaxial extension ratio , λ , is chosen as the independent parameter and all other yield criteria are tabulated in terms of it; one must of course be careful to compare yield values with yield values and fracture values with fracture values. Numerical values for these quantities characteristic of cured natural rubber are presented later in the discussion.

Some comments regarding Table I are in order. First of all, note that for the uniaxial stress field all the yield criteria with the exception of the maximum principal strain and distortion strain energy are proportional to the same factor $(\lambda^2 - \lambda^{-1})$. A similar situation holds for the equal biaxial tension case, except that the factor is $(\lambda^2 - \lambda^{-4})$. In both stress fields the ultimate stresses are simply equal to the ultimate strain times twice the shear modulus. Second, if the strains are large, all of the criteria are proportional to λ^2. One might suspect therefore that the problem of defining an ultimate criteria for an incompressible elastomer is straightforward: measure λ at yield (or fracture) in any kind of stress field, and as long as $\lambda \gtrsim 3$ the error made in failing to distinguish among them is of the order of 5 - 10%. If, however, the fracture strain is small, of the order of 20 to 30 percent as it may be in actual rocket motors, the criteria will depend upon the stress state. The similarity of the strain proportionality factor for many of the criteria implies, however, that it may be sufficient when designing experiments to contemplate testing the hypothesis in only three of the original seven of Table I, namely (i) mean deviatoric stress (stress distortion), (ii) distortion strain energy (strain distortion), and (iii) maximum principal (normal) strain, as suggested earlier in this section.

TABLE I

	Yield Criterion	Uniaxial Stress Field	Equal Stress Field	General Stress Field
1	maximum principal strain	$\lambda - 1$	$\lambda - 1$	$\lambda - 1$
2	maximum strain difference	$\frac{1}{2}\left(\lambda^2 - \frac{1}{\lambda}\right)$	$\frac{1}{2}\left(\lambda^2 - \frac{1}{\lambda^4}\right)$	$\frac{1}{2}\left(\lambda_i^2 - \lambda_j^2\right)$
3	mean deviatoric strain	$\frac{1}{2}\left(\lambda^2 - \frac{1}{\lambda}\right)$	$\frac{1}{2}\left(\lambda^2 - \frac{1}{\lambda^4}\right)$	$\frac{1}{2}\sqrt{I_1^2 - 3I_2}$
4	maximum principal stress	$\mu\left(\lambda^2 - \frac{1}{\lambda}\right)$	$\mu\left(\lambda^2 - \frac{1}{\lambda^4}\right)$	$\mu\lambda_i^2 + \overline{p_c}$
5	maximum stress difference	$\mu\left(\lambda^2 - \frac{1}{\lambda}\right)$	$\mu\left(\lambda^2 - \frac{1}{\lambda^4}\right)$	$\mu\left(\lambda_i^2 - \lambda_j^2\right)$
6	mean deviatoric stress	$\mu\left(\lambda^2 - \frac{1}{\lambda}\right)$	$\mu\left(\lambda^2 - \frac{1}{\lambda^4}\right)$	$\mu\sqrt{I_1^2 - 3I_2}$
7	distortion strain energy	$\frac{\mu}{2}\left(\lambda^2 + \frac{2}{\lambda} - 3\right)$	$\frac{\mu}{2}\left(2\lambda^2 + \frac{1}{\lambda^4} - 3\right)$	$\frac{\mu}{2}\left(I_1 - 3\right)$

As an illustration of how one might predict the ultimate values of the yield stresses and strains in equal biaxial tension and pure shear from uniaxial ultimate data represented by λ^*, consider the following calculation based upon a maximum distortion strain energy criterion.

From equations (1a), (2) and (9), we have

$$I_{1uni} = \lambda^{*2} + \frac{2}{\lambda^*} \tag{1a}$$

$$\bar{\sigma}_{uni} = \mu\left(\lambda^{*2} - \frac{1}{\lambda^*}\right) \tag{2}$$

$$W_{max} = \frac{\mu}{2}\left(I_1 - 3\right) \tag{9}$$

where λ^* is known from experiment. Now for an equal biaxial stress field, using a subscript $\underline{b}$, the first invariant is

$$I_{1b} = 2\lambda_b^2 + \frac{1}{\lambda_b^4} \tag{44}$$

whereupon equating the strain energies using (9) and the respective values of I_1, find

$$2\lambda_b^2 + \frac{1}{\lambda_b^4} = \lambda^{*2} + \frac{2}{\lambda^*}$$

One root is obviously

$$\lambda_b = \frac{1}{\sqrt{\lambda^*}}$$

which corresponds to biaxial compression and is extraneous. The other root is

$$\lambda_b = \frac{1}{\sqrt{-\frac{\lambda^*}{2} + \sqrt{(\lambda^*/2)^2 + 2/\lambda^*}}}$$

For large λ^*, we have: $\lambda_b \to \lambda^*/\sqrt{2}$, which is a useful rule of thumb for predicting biaxial failure (large strain) in a rubber when the ultimate uniaxial strain is known. Similarly, the associated stress ratio can be calculated as $\bar{\sigma}_b/\bar{\sigma}_{uni} = \frac{1}{2}$. On the other hand, for small strains such that the maximum value of the strain energy is small enough so that λ may be approximated by $1 + \epsilon$, then it follows that $\epsilon_b = \epsilon^*/2$, and $\bar{\sigma}_b = \bar{\sigma}_{uni}$ at fracture.

For the second case, pure shear generated in a material by applying the extension field

$$\lambda_x = \lambda_s \; ; \quad \lambda_y = 1 \; ; \quad \lambda_z = \lambda_s^{-1}$$

leads to

$$W = \frac{\mu}{2}\left(\lambda_s^2 - 2 + \lambda_s^{-2}\right) = \frac{\mu}{2}\frac{(\lambda_s^2 - 1)^2}{\lambda_s^2} = \frac{\mu}{2}\left(\lambda^{*2} + \frac{2}{\lambda^*} - 3\right)$$

For large λ

$$\lambda_s \approx \lambda^* - \frac{1}{2\lambda^*} \tag{45}$$

$$\frac{\sigma_s}{\sigma_{uni}} \approx \frac{\lambda^* - \frac{1}{2\lambda^*}}{\lambda^* - \frac{1}{\lambda^{*2}}} \tag{46}$$

whereas if the strains are small

$$\frac{\epsilon_s}{\epsilon_{uni}} \approx \frac{\sqrt{3}}{2} \tag{47}$$

$$\frac{\sigma_s}{\sigma_{uni}} \approx \frac{4}{3} \tag{48}$$

Returning to specific consideration of a particular unfilled elastomer, consider the fracture characteristics of gum rubber. The properties of the simple tensile curve at yield and at rupture are summarized in Table II, along with some predicted and measured values obtained for other stress distributions. In connection with these properties, a few comments can be made.

The extension ratio at yield is taken to be 6 on the basis of the discontinuity in the curve of Figure 3. The associated σ, W and σ_d are tabulated. For large strains, it is necessary to adapt a definition of the mean deviatoric strain based on finite elastic theory. It is convenient to work with Murnaghan's definition of strain:

$$\frac{1}{2}\left(\lambda_i^2 - 1\right) = \epsilon_i \tag{49}$$

so that

$$\frac{1}{2}\left(I_1 - 3\right) = \vartheta \tag{50}$$

TABLE II

Fracture Properties of an Unfilled Gum Rubber Vulcanizate

(μ = 1.76 kg/cm^2, E = 5.28 kg/cm^2, 1 kg/cm^2 = 14.22 psi)

Property	Table I Ref. Line	Failure Mode	Simple Tension	Homogeneous Biaxial Tension		Heterogeneous Triaxial Tension
λ	1	yield	6.00	*4.30	⊥6.82	6.00
σ	4	↓	12.0	7.58	12.0	4.85
W_d	7	↓	29.9	29.9	69.2	29.9
σ_d	6	↓	12.0	7.58	12.0	4.85
e_d	3	↓	17.9	17.9	44.9	17.9
λ	1	fracture	7.65	-	-	-
σ	4	↓	32.0	-	32.0	5.81
W_d	7	↓	62.4	62.4	-	-
σ_d	6	↓	32.0	-	32.0	-
e_d	3	↓	29.2	-	-	-

* energy criterion

⊥ deviatoric stress criterion

Now define the strain deviators and mean deviatoric strain by:

$$e_i = \epsilon_i - \frac{\vartheta}{3} \tag{51}$$

$$e_d = \sqrt{3/2\,(e_1^2 + e_2^2 + e_3^2)} = \frac{1}{2}\sqrt{(I_1^2 - 3I_2)} \tag{52}$$

after some algebraic manipulation. This is the last yield parameter tabulated.

Of the five chosen, most likely candidates for the yield criterion are as mentioned earlier, W, σ_d and λ. To date, the data necessary to place these quantites on a firm experimental basis have not been procured. In the meanwhile, some predictions will be made for biaxial and triaxial tension. Comparison is established with the only available multiaxial data [20].

In the first column, under the heading of biaxial tension, it is assumed that rupture occurs always at a given value of the strain energy, approximately 30 psi. Notice that it takes less biaxial stress, and of course, less biaxial strain to effect yield and presumably rupture under this assumption. If, on the other hand, the mean deviatoric stress is chosen for the yield criterion (second column), then the sample in biaxial tension fails at the same stress level as in simple tension, but at a much higher strain energy level. The calculations are carried out with the aid of (2).

The case of triaxial tension introduces some new features into the picture. In the first place, a truly incompressible material cannot deform under triaxial tension unless at least one lateral dimension is allowed to strain. This can be accomplished for example by bonding a cylindrical sample between two rigid steel plates. In this case, incompressibility of the specimen is preserved by necking of the sample. Gent and Lindley[20] subjected such poker-chip specimens to tension and found that the stress-strain curve is linear up to a point at which the sample suddenly develops an internal void; they term this the triaxial yield point. They show, to a good approximation, that the average applied stress level S' (kg/cm^2) at which the void occurs is given by

$$S' = E e' \left[1 + \frac{a^2}{2h^2}\right] = P_m' \left[\frac{1}{2} + \frac{h^2}{a^2}\right] \tag{53}$$

where e' is the strain level at yield

a is the radius of the tablet (cm)

h is the thickness of the tablet (cm)

P'_m is the maximum hydrostatic pressure acting on the yield surface just prior to yield (kg/cm^2)

For samples characterized by h/a = 0.3, they measured the yield stress for a number of rubbers and found experimentally

$$S' = 0.50 + 0.55 E = 0.59 P'_m \qquad (54)$$

by (53), so that

$$P'_m = 0.85 + 0.94 E \qquad (55)$$

Insertion of the tensile modulus of 5.28 into (55) yields the tabulated value of 5.81 kg/cm^2 for the indirectly measured triaxial stress on the yield surface just prior to yield.

It is possible to calculate how the high triaxial stress originates. Gent and Lindley assume that a tiny microscopic void is present to start with at the center of the disk. They assume further that the void is stretched radially like a spherical cavity, and they compute the stress P'_m as the point at which the cavity becomes infinitely large. This treatment can be modified for two reasons. First, when the cavity has grown large, the radially symmetric stress distribution will become distorted. Moreover, from the start the cavity is not being elongated equally in all three directions. Actually, it may be more like extension in the direction normal to the flat specimen with zero displacement in the two transverse directions. Since such a displacement field is impossible for a cavity in an incompressible medium, however, it may be assumed that the cavity is a small cylinder, lying with its axis perpendicular to the pull direction, and being stretched radially with its axial length held fixed. This will be closer to reality than the case of the spherical cavity. The solution of this problem is a classical case in finite elastic theory [15] the details of which need not concern us here.

Suffice it to point out that the radial stress in the medium around the cavity is given by

$$\frac{\overline{\sigma_r}}{\mu} = \ln\left(\frac{\lambda_a}{\lambda}\right) + \frac{1}{\lambda^2} - \frac{1}{\lambda_a^2} \tag{56}$$

where the bar over the stress symbol indicates true stress and

λ is the radial extension ratio $= \frac{1}{r}\sqrt{\bar{a}^2 - a^2 + r^2}$

a is the radius of the undeformed cavity.

Far away from the cavity, $\lambda \to 1$ and the stress approaches P_m'.

$$\frac{P_m'}{\mu} = \ln \lambda_a + 1 - \frac{1}{\lambda_a^2} \tag{57}$$

Likewise, the tangential stress at the surface of the cavity is given by

$$\left(\frac{\overline{\sigma_\theta}}{\mu}\right)_a = \lambda_a^2 - \frac{3}{2\lambda_a^2} \tag{58}$$

which, for $\lambda \gtrsim 3$, behaves exactly like simple tension; this checks the facts because the surface of the cylinder is assumed to stretch tangentially, but not axially. On this basis, we choose the yield value for λ_a to be that in simple tension, namely 6.00. Substitution into (57) yields for P_m' a value of 4.85 kg/cm^2 (tabulated under the heading σ at yield), in excellent agreement with the measured value. Furthermore, it is to be expected that the measured value will be higher since it is a measured break rather than yield.

The first strain invarient under the radial stretching of the cylinder is given by

$$I_1 = \lambda_a^2 + 1 + \frac{1}{\lambda_a^2} \tag{59}$$

so that using (9)

$$W_d = \frac{\mu}{2}\left(\lambda_a^2 + 1 + \frac{1}{\lambda_a^2} - 3\right) \doteq 0.883\,(34.0) = 29.9 \tag{60}$$

Thus the strain energy remains constant as in simple tension. With admittedly only fragmentary evidence it appears that it may not be a poor assumption to take W_d as the yield criterion. In this particular case, the criterion states that this particular gum rubber vulcanizate cannot sustain more than 30 kg/cm^2 or 425 in-lbs/in^3 of strain energy density without yielding. It is suggested, however, that similar experiments to those of Gent and Lindley in both tension and compression be expedited to provide the data needed to define the yield criterion.

b. Illustrative example:- On the basis of the suggestion made in the previous section, it seems appropriate to apply the strain energy criterion to a practical problem in order to demonstrate its use. In the strict sense of the word, finite elastic theory should be used, but since not many design engineers have familiarized themselves with the intricacies of this treatment, an analysis based on infinitesimal theory will first be presented. We consider the classical case of pressurization of an infinitely long hollow bonded cylinder in an elastic case. Since the nomenclature from hereon is familiar, interjections will be sparse. Superscript bar refers to properties of the metal case. Using (9) in the form

$$W_d = \frac{2}{3}\mu\left[\left(\frac{du}{dr}\right)^2 - \frac{u}{r}\frac{du}{dr} + \left(\frac{u}{r}\right)^2\right] \tag{61}$$

with p as the internal pressure, one finds upon the appropriate substitution that at the inner surface

$$W_d = \frac{P^2}{6\mu}\,\frac{(1-2\nu)^2(a/b)^2(1-\phi)^2 + 3(1+\phi-2\nu)^2}{\left[1+\phi-2\nu+(a/b)^2(1-\phi)\right]^2} \tag{62}$$

where $\phi = \frac{\mu}{\bar{\mu}}\left[1-(3-2\bar{\nu})/S\right]$ is the effective case rigidity.

For an infinitely stiff case, for example, and typical large web fractions,

$$P_{max} \approx 30\sqrt{W_d} \tag{63}$$

which upon using $W_d = (\mu/2)(I_1 - 3)$ from Table II, gives a maximum internal allowable pressure of 170 psi. Figure 16 shows how W_d varies with Poisson's ratio for the particular case when $\phi = 0.004$, $a/b = 0.25$ and $p = 1000$ psi. Note that W_d increases very rapidly as ν falls below $\frac{1}{2}$. The need for such a large strain energy will in part be eased by relaxation effects in the propellant. But a very important reason that results in these high values lies in the error made by assuming small strain theory out to rupture. The error made is akin to assuming that the initial slope of the tensile curve remains constant to rupture . Thus the value of 900 psi is not to be treated as universal, particularly when large strains are involved. On the other hand, calculations of this sort based on small strain theory do become more meaningful at low temperatures. There the stress-strain curve does become linear, while the ratio of μ to $\bar{\mu}$ increases, as does the relative case rigidity effect.

Because it is extermely important to be able to apply the strain energy criterion to practical cases, the finite elastic analysis of the infinitely long internally pressurized cylinder is carried out in Appendix 5. 3 in order to show the large error engendered by small strain theory. Actually, the analysis is merely an extension of the results that were presented for the cavity. In order to keep the analysis fairly simple, it is necessary to assume incompressibility. The analysis can be carried out for a compressible material with a bit more difficulty, but for present propellant materials, a representative strain energy density function is not available.

The result given for the assumed incompressible material

$$W_d = \frac{p^2\phi}{2[(a/b)p\phi + \mu(a/b)^2]} \tag{63}$$

$$\frac{p}{\mu} = \frac{(a/b)^2(\lambda_a^2 - 1)}{\phi} \tag{64}$$

which is the large strain analog to (62). For small case rigidities,

$$W_d \approx \frac{p\phi}{2(a/b)^2} \tag{65}$$

and it is easily seen by comparing (62) and (65) that the energy increases quadratically with pressure in small strain theory, but for large strains approaches a linear asymptote in pressure.

Thus this illustrative calculation demonstrates that if the strains are large, much lower demands will be placed upon the allowable strain energy than were indicated by, for example, the 900 psi figure obtained by extrapolating the small strain theory.

4. Filled elastomers

Returning now to the practical problem of rocket grain analysis, it is clear that fracture prediction will not be nearly as simple for highly filled elastomers or propellants, since the materials are compressible and yield at strains as low as 20 percent ($\lambda = 1.20$) where as can be seen from Table I, the criteria depend upon the stress state.

a. Possible fracture criteria:- It has been suggested that, in the case of unfilled elastomers, the distortion strain energy adequately represents the onset of fracture or yield . In the case of filled elastomers, two factors complicate the situation; one deals with the cutting of the polymer chains on the sharp edges of the filler engendered by the high local stresses around the particles, the other is the generation of voids as the binder is pulled away from the filler. One simple modification to the strain energy function to account for these factors can be proposed.

The first modification deals with the cutting of polymer chains. This inference is borne out by constant strain test data (i) as strain is increased, time to rupture decreases, (ii) at a given strain, the modulus decreases with time. Thus, from stress relaxation studies at various strain levels, it is possible to correlate the modulus with some function of time and strain level and also temperature. The strain energy criterion now becomes:

$$W = \frac{1}{2}\mu(t, \lambda, T)\left[I_1 - 3\right] \tag{66}$$

Secondly, the void volume must be accounted for since the strain energy is defined per unit volume of unstrained material. If β is the void fraction engendered by pullaway at a given λ, then (66) becomes

$$W_d = \frac{1}{2}\mu(t,\lambda,\tau)\left[I_1 - 3\right]\cdot\left[1 - \beta(\lambda)\right] \qquad (67)$$

where W_d is now measured on the sample including voids. Measurements of void volumes can be done microscopically on thin films.

Until more definitive data becomes available no attempt will be made to present an example of typical calculations using actual propellant material properties.

F. Cumulative Damage Theory

In any discussion of failure theory, it is necessary to show the correlation between experimental data accumulated at constant strain rates, and actual test and environmental conditions wherein the strain rate may change slow or fast during the time under consideration. It has already been proposed in the third progress report that one may use a cumulative damage concept similar to that used in fatigue analysis to account for the amount or percentage of resistance to failure used up as the strain rate takes on various values during the loading cycle.

Since the proposal in that report, McCullough has had occasion to run a series of preliminary room temperature tests to fracture on tensile specimens in an Instron tester at constant and mixed strain rates. The degree of correlation obtained has been somewhat encouraging even though limited. It shows cumulative damage tests only 15 to 20 percent different from predictions based on constant rate data, with the standard deviation being somewhat lower for a strain rather than energy basis of correlation.

Further remarks along these lines will also be withheld until a later time.

APPENDICES

APPENDIX 5.1 - Stress Analysis of a Thin Clamped Disk

In the course of analyzing failure characteristics of propellant specimens, it was indicated that one could test under essentially hydrostatic tension conditions by cementing a thin disk, or poker chip, of the material between two rigid (steel) supports and exerting tension in a direction perpendicular to the faces. Under such loading, the center of the specimen would be subjected to a three-dimensional tensile stress. The elementary analysis of the problem, assuming the disk radius is infinite such that plane strain conditions hold, leads to the result that the radial and circumferential stresses are equal and, for an isotropic homogeneous medium with Poisson ratio, ν, proportional to the applied axial stress σ_z.

$$\sigma_r = \sigma_\theta = \frac{\nu}{1-\nu}\sigma_z \qquad (1)$$

It may be noted that for an incompressible material not only is the stress state triaxial, but it is also hydrostatic leading to there being no shear distortion in the specimen.

Coupon tests have been employed by Gent and Lindley [20] in their experiments upon rubber and by Lehrer and Schwalzbart* in metals. The purpose of the following analysis is to calculate the stress distribution in a compressible thin disk of finite radius.

Gent and Lindley were primarily concerned with displacements and in their analysis employed what was equivalent to a minimum potential energy solution to predict deformations and an apparent modulus. However, for their approximation, a variational procedure was not used because the only free constant in their analysis, the amplitude of the assumed parabolic deformation or bulge, was fixed by the condition of incompressibility. While it would be straightforward to extend their analysis by introducing a higher order deformation shape and provision for compressibility, it does not seem warranted at this time because our current interest is concerned with stresses.

---

* Static and Fatigue Strength of Metals Subjected to Triaxial Stresses" Institute of the Aeronautical Sciences paper no. 60-12, January 1960.

Complementary energy analysis

The stress analysis will be carried out using the minimum complementary energy principle for a disk of thickness 2h and unit radius. The faces $z = \pm h$ are assumed to be rigidly bonded to much stiffer supporting plates. We may therefore formulate the problem, assuming circumferential symmetry, as requiring the satisfaction of the field equations of equilibrium

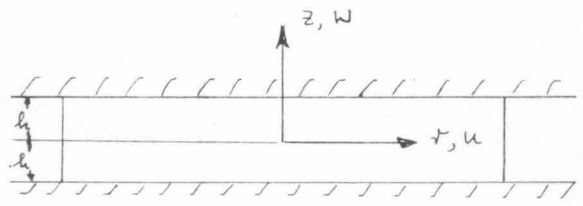

$$\frac{\partial \sigma_r}{\partial r} + \frac{\sigma_r - \sigma_\theta}{r} + \frac{\partial \tau_{rz}}{\partial z} = 0 \qquad (2)$$

$$\frac{\partial \tau_{rz}}{\partial r} + \frac{\tau_{rz}}{r} + \frac{\partial \sigma_z}{\partial z} = 0 \qquad (3)$$

and compatibility

$$\left(\frac{\partial^2}{\partial r^2} + \frac{1}{r}\frac{\partial}{\partial r} + \frac{\partial^2}{\partial z^2}\right)\sigma_r - \frac{2(\sigma_r - \sigma_\theta)}{r^2} + \frac{1}{1+\nu}\frac{\partial^2 \Theta}{\partial r^2} = 0 \qquad (4)$$

$$\left(\frac{\partial^2}{\partial r^2} + \frac{1}{r}\frac{\partial}{\partial r} + \frac{\partial^2}{\partial z^2}\right)\sigma_\theta + \frac{2(\sigma_r - \sigma_\theta)}{r^2} + \frac{1}{1+\nu}\frac{\partial \Theta}{\partial r} = 0 \qquad (5)$$

$$\left(\frac{\partial^2}{\partial r^2} + \frac{1}{r}\frac{\partial}{\partial r} + \frac{\partial^2}{\partial z^2}\right)\sigma_z + \frac{1}{1+\nu}\frac{\partial^2 \Theta}{\partial z^2} = 0 \qquad (6)$$

$$\left(\frac{\partial^2}{\partial r^2} + \frac{1}{r}\frac{\partial}{\partial r} + \frac{\partial^2}{\partial z^2}\right)\tau_{rz} - \frac{\tau_{rz}}{r^2} + \frac{1}{1+\nu}\frac{\partial^2 \Theta}{\partial r \partial z} = 0 \qquad (7)$$

where $\Theta \equiv \sigma_r + \sigma_\theta + \sigma_z$. The boundary conditions are on the faces

$$u(r, \theta, \pm h) = v(r, \theta, \pm h) = 0 \qquad (8)$$

$$w(r, \theta, \pm h) = \pm w_0 \tag{9}$$

and on the unloaded circumference

$$\sigma_r(1, \theta, z) = \tau_{rz}(1, \theta, z) = 0 \tag{10}$$

The elasticity solution to this problem is a formidable one which is the reason for using an energy approach. The theorem of minimum complementary energy requires* that a proposed stress state is admissible if

a) it satisfies the stress equations of equilibrium
b) the boundary conditions on that part of the boundary where stresses are prescribed.

Inspection of (2)-(7), and (8)-(10) indicates by implication that the compatibility equations may not necessarily be satisfied, nor may the displacement boundary conditions (8) and (9). The theorem however guarantees that if there is some arbitrariness in the proposed stress state, it may be adjusted by minimizing the complementary energy

$$V^* = \int_{-h}^{h}\int_{0}^{2\pi}\int_{0}^{1}\left\{\frac{1}{2E}\left[\sigma_r^2+\sigma_\theta^2+\sigma_z^2\right] - \frac{\nu}{E}\left[\sigma_r\sigma_\theta + \sigma_\theta\sigma_z + \sigma_z\sigma_r\right] + \frac{1}{2G}\tau_{rz}^2\right\} r\,dr\,d\theta\,dz - 2\int_{0}^{2\pi}\int_{0}^{1}\sigma_z(r,h)\,w_0\,r\,dr\,d\theta \tag{11}$$

to give the best possible averaged satisfaction of the compatibility and displacement boundary conditions.

The heart of the problem lies in the initial choice of the admissible functions which is accomplished mainly by intuition and experience. Without any rationalization at this time, consider the following set which was chosen for reasonable simplicity in the subsequent algebra required.

$$\sigma_r = \frac{2\nu}{1-\nu} A\left[1 - r^n\right] \cosh\sqrt{\frac{2\nu}{1-\nu}}\, z \tag{12}$$

$$\sigma_\theta = \frac{2\nu}{1-\nu} A\left[1-(n+1)r^n + r^{p+1} - r^2\right] \cosh\sqrt{\frac{2\nu}{1-\nu}}\, z \tag{13}$$

---

* See Sokolnikoff, Mathematical Theory of Elasticity, McGraw Hill, 1956.

$$\sigma_z = \sigma_o + \left[1 - \frac{p+1}{2} r^{p-1}\right]\left[2A \cosh\sqrt{\frac{2\nu}{1-\nu}}\, z - \sigma_o\right] \tag{14}$$

$$\tau_{rz} = -A\left[r - r^p\right]\sqrt{\frac{2\nu}{1-\nu}} \sinh\sqrt{\frac{2\nu}{1-\nu}}\, z \tag{15}$$

It will be found upon substitution into (2) and (3) that the equilibrium equations are satisfied, whereas insertion of r = 1 into (12) and (15) satisfy (10). The function set is therefore admissible, and furthermore contains a degree of arbitrariness represented by the, at present, unknown constants σ_o, A, p, and n. These latter constants will be determined by minimizing V*, e.g. $\partial V^*/\partial \sigma_o = 0$, etc.

In passing it may be noted that the exponents n and p must exceed 0 and 1 respectively in order that infinite stresses are not introduced at the origin. Also the set has been chosen in such a way that at the origin r = z = 0,

$$\sigma_r = \sigma_\theta = \frac{\nu}{1-\nu}\sigma_z \tag{1}$$

to yield the desired limit as the disk thickness approaches zero, or, what is the same, the radius of the disk becomes infinitely large. Finally σ_o, although unknown, may be identified as the average tensile stress acting on the face to cause the deformation w_o.

For convenience, we define

$$\mu^2 = \frac{2\nu}{1-\nu} \tag{16}$$

and proceed to insert (12)-(15) into (11) to obtain the complementary energy as a function of the parameters, V* = V*(A, σ_o, n, p). After the intergration and algebraic reduction, there results

$$\frac{E}{\pi} V^* = (S_1 + S_2 - 2\nu S_4)\, t_1 + S_3 t_2 - 2\nu S_5 t_3 + 2(1+\nu) S_6 t_4 \tag{17}$$
$$+ \sigma_o^2 h - 2E w_o \sigma_o + \mu\nu A \sigma_o \left(\frac{p-1}{p+3}\right) \sinh \mu h$$

Where the following notation has been employed

$$S_1 = \frac{n^2}{2(n+1)(n+2)}$$

$$S_2 = 2(n+1)\left[\frac{n(n+6)}{4(n+2)(n+4)} - \frac{1}{n+p+3}\right] + \frac{p+15}{6(p+3)} - \frac{3(p+1)}{2(p+2)(p+5)}$$

$$S_3 = \frac{(p-1)^2}{2p}$$

$$S_4 = -\frac{n(p-1)(n+p+7)}{4(p+3)(n+p+3)(n+4)}$$

$$S_5 = \frac{n(p-1)}{p+n+1}$$

$$S_6 = \frac{(p-1)^2}{4(p+3)(p+1)}$$

$$t_1 = \frac{\mu^3 A^2}{2}\left[\sinh 2\mu h + 2\mu h\right]$$

$$t_2 = \frac{A^2}{2\mu}\left[\sinh 2\mu h + 2\mu h\right] - \frac{2\sigma_0 A}{\mu}\sinh \mu h + \sigma_0^2 \frac{h}{2}$$

$$t_3 = \frac{\mu A^2}{2}\left[\sinh 2\mu h + 2\mu h\right] - \sigma_0 A \mu \sinh \mu h$$

$$t_4 = \frac{\mu A^2}{2}\left[\sinh 2\mu h + 2\mu h\right]$$

The minimizing condition $\partial V^* / \partial A = 0$ leads to

$$A = \frac{\left[2S_3 - 2\nu S_5 \mu^2 - \nu \mu^2 \frac{p-1}{p+3}\right]\sigma_0 \sinh \mu h}{\left[(S_1 + S_2 - 2\nu S_4)\mu^4 + S_3 - 2\nu \mu^2 S_5 + 2(1+\nu)\mu^2 S_6\right]\left[\sinh 2\mu h + 2\mu h\right] - 8(1+\nu)\mu^3 h S_6} \qquad (28)$$

while $\partial V^*/\partial \sigma_o = 0$ in conjunction with (28) gives

$$\sigma_o = \frac{\frac{Ew_o}{h}}{1 + \frac{S_3}{2} - \frac{[2S_3 - (2S_5 + \frac{p-1}{p+3})\nu\mu^2]^2 \sinh^2 \mu h}{2\mu h\{[(S_1+S_2-2\nu S_4)\mu^4 + S_3 - 2\nu\mu^2 S_5 + 2(1+\nu)\mu^2 S_6][\sinh 2\mu h + 2\mu h] - 8\mu^3 h(1+\nu)S_6\}}} \tag{29}$$

which value of σ_o can be inserted into (28) to determine $A = A(w_o)$. With A and σ_o known as functions of (n, p, w_o), they can be inserted into (17) to find

$$V^* = V^*(n, p; w_o) \tag{30}$$

In principle, therefore, one could add the additional minimizing conditions $\partial V^*/\partial n = 0$ and $\partial V^*/\partial p = 0$ and find finally n and p as functions of the applied deformation w_o and of course the thickness parameter h. Hence, all the constants A, σ_o, n, and p are known in terms of w_o and h and can be placed back into the stress distribution (12)-(15) to give the final approximate stresses.

From the algebraic standpoint, however, it proves simpler to try various values of n_i and p_j in (30) and compute the corresponding value of V*. There will be some pairs that will give the algebraic minimum by this trial and error procedure which is equivalent to applying the minimizing conditions.

At this stage in the analysis, it is worth reëxamining the necessity for finding this stress distribution with due consideration to the computational work involved. At least one solution is now available, but it may be worth investigating other function sets to see if they may be computationally simpler. Furthermore, it is recommended that any computations be first carried out for an incompressible medium, $\nu = \frac{1}{2}$, $\nu\mu^2 = 1$.

If additional work on this solution or variations of it are thought warranted, it will be reported at a later time. The only qualitative statement which can be made at this time is that the true values of n, p will probably

be fairly large corresponding to a stress distribution fairly close to (1) over a large part of the central portion of the disk. One major limitation of the technique is that both n and p will depend upon the width/thickness ratio of the sample, so that a parameter study of the latter ratio would entail an iteration of the computation of n and p.

APPENDIX 5.2 - Crack Propagation in Viscoelastic Media

In the body of the report, the stress distribution near a small crack in a large thin sheet subjected to a uniform tensile stress was discussed. Further, it was pointed out that the viscoelastic and elastic stress distributions are the same for this loading, thus leading to the possibility of computing the viscoelastic strains and displacements from the basic elastic information. The purpose of the following analysis is to use this information to predict crack propagation characteristics in a viscoelastic medium.

From the basic solution [26] the biaxial stress distribution in the plate strip subjected to a tension σ_o is

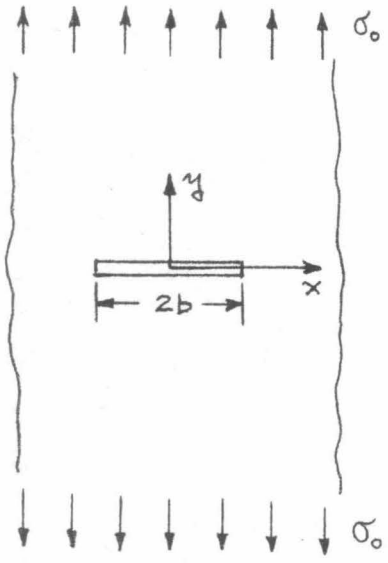

FIG. 5.2 a

$$\sigma_x(x,0) = \frac{\sigma_o b^2}{\sqrt{x^2-b^2}\left[x+\sqrt{x^2-b^2}\right]} \; ; \qquad x>b \qquad (1\text{-a})$$

$$= \sigma_o\left\{\sqrt{\frac{1}{2\epsilon}} - 1 + O\left[\left(\frac{\epsilon}{b}\right)^{\frac{1}{2}}\right] + \cdots\right\} ; \quad x = b+\epsilon \qquad (1\text{-b})$$

$$\sigma_y(x,0) = \sigma_o\left\{1+\frac{b^2}{\sqrt{x^2-b^2}\left[x+\sqrt{x^2-b^2}\right]}\right\} ; \quad x>b \qquad (2\text{-a})$$

$$= \sigma_o\left\{\sqrt{\frac{1}{2\epsilon}} + O\left[\left(\frac{\epsilon}{b}\right)^{\frac{1}{2}}\right]\right\} ; \qquad x = b+\epsilon \qquad (2\text{-b})$$

where it is clear that the stress becomes infinite as the point of the crack is approached. In order to circumvent the necessity for conducting a large strain, elasto-plastic solution, it will arbitraily be assumed that the stress may build up to a specified value at a distance δ from the crack tip and remain constant throughout the interval $0 \leq x-b \leq \delta$ until an ultimate one-dimensional strain ϵ^* is reached.

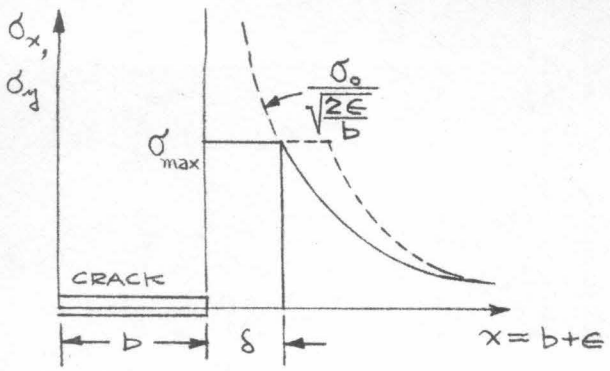

FIG. 5.2 b

It should be observed that the elastic solution is no longer correct, because the specimen, by the equations of equilibrium, is presumed to be absorbing the stress indicated by the dashed line. Thus the load represented by integrating the stress between x = b and x = b + δ is not accounted for when the truncation is made. Therefore the actual stress distribution would be more like the dotted line, with the additional area accomplishing the necessary force balance. On the other hand, because this (dotted)distribution cannot easily be calculated, and because it is desirable to still have the force balance, the analysis will be carried out using the modified truncated stress distribution shown in Figure 5.2-c on which areas A_1 and A_2 are equal. If the existence of such quantities as $\in^*$ and δ can be established by experiment, then the following analysis could lead to useful results.

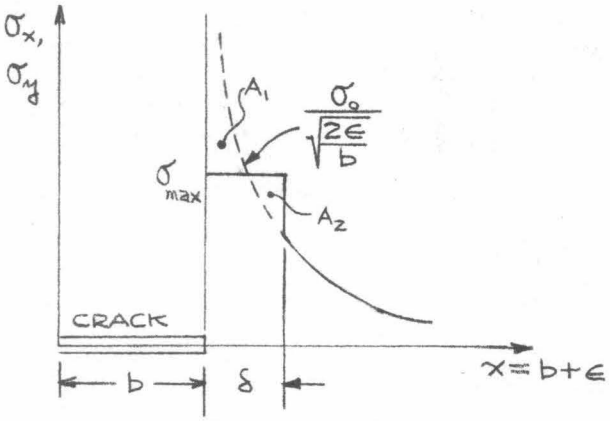

FIG. 5.2 C

Visualize then, the conditions along the line of crack prolongation, and assume that the internal forces along the shear free line are carried, for simplicity, by a series of discrete Voigt elements averaged over the characteristic length δ. The mechanism postulated is that each element will strain as a result of stresses (σ_x and σ_y) which are constant over the length δ assigned to each element as shown in Figure 5.2-d. The valuesof these stresses are determined from equations (1) and (2) and the equilibrium condition discussed earlier. Namely we assume that for a crack width 2b, the stresses acting on element (n) are the average values:

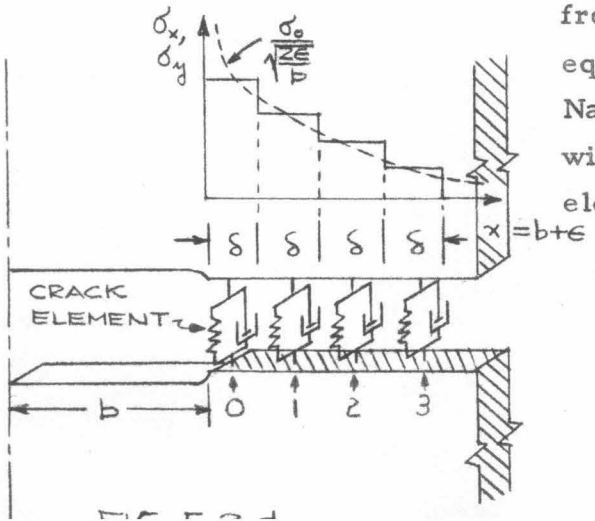

$$\frac{\sigma_{nx}}{\sigma_o} = \frac{1}{\delta}\int_{b+n\delta}^{b+(n+1)\delta} \frac{\sigma_x(x)}{\sigma_o}\,dx = \frac{b^2}{\delta}\int_{b+n\delta}^{b+(n+1)\delta} \frac{dx}{\sqrt{x^2-b^2}\,[x+\sqrt{x^2-b^2}]}$$

$$\simeq \frac{2}{\sqrt{2\,\delta/b}}\left[(n+1)^{\frac{1}{2}} - n^{\frac{1}{2}}\right] - 1 + \frac{1}{4}\sqrt{\frac{2\delta}{b}}\left[(n+1)^{\frac{3}{2}} - n^{\frac{3}{2}}\right] + \frac{2\,\delta/b}{2}\left[(n+1)^2 - n^2\right] + \cdots \quad (3\text{-a})$$

$$\frac{\sigma_{ny}}{\sigma_o} = \frac{1}{\delta}\int_{b+n\delta}^{b+(n+1)\delta} \frac{\sigma_y(x)}{\sigma_o}\,dx = \frac{1}{\delta}\int_{b+n\delta}^{b+(n+1)\delta} \left\{1 + \frac{b^2}{\sqrt{x^2-b^2}\,[x+\sqrt{x^2-b^2}]}\right\} dx \quad (3\text{-b})$$

$$\simeq \frac{2}{\sqrt{2\,\delta/b}}\left[(n+1)^{\frac{1}{2}} - n^{\frac{1}{2}}\right] + \frac{1}{4}\sqrt{\frac{2\delta}{b}}\left[(n+1)^{\frac{3}{2}} - n^{\frac{3}{2}}\right] + \frac{2\,\delta/b}{2}\left[(n+1)^2 - n^2\right] + \cdots$$

After the strain in the first element reaches ϵ^*, it will break and the stress distribution will shift by one δ width; i.e., the stress which had been acting on the element n is now acting on element n + 1, where the effective crack length to be used is 2 (b + δ). After m translations, or after element (m - 1) breaks, one has

$$\frac{\sigma_{ny}^{(m)}}{\sigma_o} = \frac{2}{\sqrt{2\delta/(b+m\delta)}}\left[(n-m+1)^{\frac{1}{2}} - (n-m)^{\frac{1}{2}}\right] + \frac{1}{4}\sqrt{\frac{2\delta}{b+m\delta}}\left[(n-m+1)^{\frac{3}{2}} - (n-m)^{\frac{3}{2}}\right] + \cdots \quad (4\text{-a})$$

$$= \frac{\sigma_{nx}^{(m)}}{\sigma_o} + 1$$

To reiterate, $\sigma_{ny}^{(m)}$ is the average stress acting on element (n) before element (m) breaks, but after element (m-1) has parted. Thus, the stress at the crack tip is given approximately by

$$\sigma_{my}^{(m)} \cong \frac{2\sigma_o}{\sqrt{\frac{2\delta}{b+m\delta}}} \cong \sigma_{mx}^{(m)} + \sigma_o \quad (4\text{-b})$$

It is clear that if δ is assumed to be a fixed characteristic dimension, the stress acting on the element at the crack tip is not limited, but increases with crack length. However, in the initial stages of crack growth ($m\,\delta \ll b$) the stress is practically constant as seen from equation (4-b).

Since we now have the two-dimensional stresses as a function of crack position, the time dependent strain in each element can be found from the plane stress, stress-strain equation. For an elastic material, we have

$$\epsilon_y = \frac{1}{E}(\sigma_y - \nu\,\sigma_x) \quad (5)$$

For simplicity we will assume an incompressible medium ($\nu = \frac{1}{2}$). The viscoelastic strain is obtained in the usual manner by replacing E by its equivalent differential operator, which for a Voigt model is [1]

$$E \rightarrow E_v \left(\tau \frac{d}{dt} + 1 \right) \tag{6}$$

where

E_v = modulus of the spring in parallel with a dashpot with viscosity η

$\tau = \frac{\eta}{E_v}$ = retardation time of model

Insertion of (6) into (5) yields the viscoelastic stress-strain equation which applies to each element

$$\tau \frac{d\epsilon_y}{dt} + \epsilon_y = \frac{1}{E_v}\left[\sigma_y - \frac{1}{2}\sigma_x \right] = \frac{1}{2E_v}\left[\sigma_y + \sigma_o \right] \tag{7}$$

In terms of the notation used in equation (4), equation (7) becomes

$$\tau \frac{d\epsilon_n^{(m)}}{dt} + \epsilon_n^{(m)} = \frac{\sigma_o}{2E_v}\left[\frac{\sigma_{ny}^{(m)}}{\sigma_o} + 1 \right] \tag{8}$$

where $\epsilon_n^{(m)}$ is the strain in element (n) before element (m) breaks, but after element (m-1) has parted. If we denote the time at which element (m) breaks by t_m, then equation (8) applies to the time interval $t_{m-1} \leq t \leq t_m$. In this time interval the right hand side of (8) is constant so that we can integrate it for the strain:

$$\epsilon_n^{(m)}(t) = \frac{\sigma_o}{2E_v}\left[\frac{\sigma_{ny}^{(m)}}{\sigma_o} + 1 \right] + \left[\epsilon_n^{(m-1)b} - \frac{\sigma_o}{2E_v}\left(\frac{\sigma_{ny}^{(m)}}{\sigma_o} + 1 \right) \right] e^{-\frac{t - t_{m-1}}{\tau}} \tag{9}$$

$$t_{m-1} \leq t \leq t_m$$

where $\epsilon_n^{(m-1)b}$ is defined as the strain existing in element (n) at the time element (m-1) breaks, which is t_{m-1}. If we set $t = t_{m-1}$ in equation (9), the initial condition

$$\epsilon_n^{(m)}(t_{m-1}) = \epsilon_n^{(m-1)b}$$

is satisfied. Letting $t \to \infty$, we have

$$\epsilon_n^{(m)}(\infty) \equiv \epsilon_{ne}^{(m)} = \frac{\sigma_o}{2E_\nu}\left[\frac{\sigma_{n\gamma}^{(m)}}{\sigma_o} + 1\right] = \frac{\sigma_o}{E_\nu}\left\{\frac{1}{\sqrt{\frac{2\delta}{b+m\delta}}}\left[(n-m+1)^{\frac{1}{2}} - (n-m)^{\frac{1}{2}}\right]\right.$$
$$\left. + \frac{1}{2} + \frac{1}{8}\sqrt{\frac{2\delta}{b+m\delta}}\left[(n-m+1)^{\frac{3}{2}} - (n-m)^{\frac{3}{2}}\right] + \cdots\right\} \tag{10}$$

which is the long-time or equilibrium strain that would result if element (m) did not break. It is seen from equation (10) that this is a known value if the crack position is given. Therefore as a matter of convenience we shall write (9) as

$$\epsilon_n^{(m)} \equiv \epsilon_{ne}^{(m)} + \left[\epsilon_n^{(m-1)b} - \epsilon_{ne}^{(m)}\right] e^{-\frac{t - t_{m-1}}{\tau}} \qquad t_{m-1} \le t \le t_m \tag{11-a}$$

and the strain at the time when element m breaks

$$\epsilon_n^{(m)b} = \epsilon_{ne}^{(m)} + \left[\epsilon_n^{(m-1)b} - \epsilon_{ne}^{(m)}\right] e^{-\frac{t_m - t_{m-1}}{\tau}} \tag{11-b}$$

This expression can now be used to calculate the time at which each element breaks and hence will give the crack velocity as a function of time.

Consider first the strain in element zero for $0 \le t \le t_o$, so that n = m = 0 and

$$\epsilon_o^{(o)} = \epsilon_{oe}^{(o)} + \left[\epsilon_o^{(-1)b} - \epsilon_{oe}^{(o)}\right] e^{-\frac{t - t_{-1}}{\tau}}$$

in which we must define $t_{-1} = 0$, $\epsilon_o^{(-1)b} = 0$ to satisfy the initial condition that the material is unstrained at t = 0. Hence

$$\epsilon_o^{(o)} = \epsilon_{oe}^{(o)}\left[1 - e^{-\frac{t}{\tau}}\right]$$

element (0) breaks at $t = t_o$ when $\epsilon_o^{(0)}(t_o) \equiv \epsilon_o^{(0)b} = \epsilon^*$,

$$\epsilon^* = \epsilon_o^{(o)b} = \epsilon_{oe}^{(o)}\left[1 - e^{-\frac{t_o}{\tau}}\right] \tag{12}$$

Solving for t_o,

$$\frac{t_o}{\tau} = -\ln\left[1 - \frac{\epsilon^*}{\epsilon_{oe}^{(o)}}\right] \tag{13}$$

which is the time that elapses before the crack starts to run. From equation (10)

$$\epsilon_{oe}^{(o)} = \frac{\sigma_o}{2E_\nu}\left[\frac{\sigma_{oy}^{(o)}}{\sigma_o} + 1\right]$$

$$= \frac{\sigma_o}{E_\nu}\left\{\frac{1}{\sqrt{2\delta/b}} + \frac{1}{2} + \frac{1}{8}\sqrt{\frac{2\delta}{b}} + \cdots\right\}$$

assuming $\left(\frac{\delta}{b}\right) \ll 1$,

$$\frac{t_o}{\tau} \cong -\ln\left[1 - \frac{\epsilon^*\sqrt{\frac{2\delta}{b}}}{(\sigma_o/E_\nu)}\right] \tag{14}$$

Equation (11) gives the strain in the next element at $t = t_1$ as

$$\epsilon_1^{(1)b} = \epsilon_{1e}^{(1)} + \left[\epsilon_1^{(o)b} - \epsilon_{1e}^{(1)}\right] e^{-\frac{t_1 - t_o}{\tau}} \equiv \epsilon^* \tag{15}$$

In order to find t_1, $\epsilon_1^{(o)b}$ must be determined from (11-b) and (12)

$$\epsilon_1^{(o)b} = \epsilon_{1e}^{(o)}\left[1 - e^{-\frac{t_o}{\tau}}\right] = \frac{\epsilon_{1e}^{(o)}}{\epsilon_{oe}^{(o)}}\epsilon^*$$

Inserting this expression in (15) and solving for t_1,

$$\frac{t_1}{\tau} = \frac{t_o}{\tau} - \ln\left\{\frac{\epsilon^* - \epsilon_{1e}^{(1)}}{\frac{\epsilon_{1e}^{(o)}}{\epsilon_{oe}^{(o)}}\epsilon^* - \epsilon_{1e}^{(1)}}\right\} = \frac{t_o}{\tau} + \ln\left\{1 + \frac{\epsilon^*\left[1 - \epsilon_{1e}^{(o)}/\epsilon_{oe}^{(o)}\right]}{\epsilon_{1e}^{(1)} - \epsilon^*}\right\} \tag{16}$$

It is observed that all of the strains appearing are equilibrium values and are thus known from equation (10). By assuming that the strain ϵ^* at which the element breaks is much smaller than the equilibrium strain $\epsilon_{1e}^{(1)}$, or equivalently that the retardation time τ is much larger than the time interval $t_1 - t_o$, equation (16) simplifies to

$$\frac{t_1}{\tau} \cong \frac{t_o}{\tau} + \frac{\epsilon^*}{\epsilon_{1e}^{(1)}}\left[1 - \frac{\epsilon_{1e}^{(o)}}{\epsilon_{oe}^{(o)}}\right]$$

Using (10) and assuming $\frac{\delta}{b} \ll 1$, it is found that

$$\frac{t_1}{\tau} = \frac{t_0}{\tau} + \frac{\epsilon^* \sqrt{2\delta/b}\,(2-\sqrt{2})}{(\sigma_0/E_y)} \tag{17}$$

The initial velocity of crack propagation is given by

$$v_1 = \frac{\delta}{t_1 - t_0} = \frac{\delta/\tau}{\frac{t_1 - t_0}{\tau}}$$

and from (17) is approximately

$$v_1 \cong \frac{\sigma_0/E_y \sqrt{b\delta}}{\tau \epsilon^* 2(\sqrt{2}-1)} \tag{18}$$

As a rough means of estimating δ , consider McCullough's preliminary data[25] Figure 15 in the region of constant stress, from which $V \approx 2 \times 10^{-3}$ in/sec, $\sigma_0 = 20$ psi, b = 0.2 inches. Using typical room temperature properties gives $\delta \approx 10^{-3}$ inches, which does not seem to be an unreasonable magnitude and may be thought of as a characteristic strand diameter. Note, as hypothesized $\delta/b \ll 1$

Calculation of crack tip velocity as a function of tip location. -

With these results appearing reasonable, it is appropriate to extend the analysis and obtain an expression for crack tip velocity as a function of crack growth. To do this, the expression (11-b) for $\epsilon_n^{(m)b}$ must first be expanded so that all of the strains which appear on the right hand side are the known equilibrium values. It is seen from (11-b) that $\epsilon_n^{(m-1)b}$ must be replaced by a function of equilibrium strains. If we write

$$\epsilon_n^{(m-1)b} = \epsilon_{ne}^{(m-1)} + \left[\epsilon_n^{(m-2)b} - \epsilon_{ne}^{(m-1)}\right] e^{-\frac{t_{m-1} - t_{m-2}}{\tau}}$$

it is seen that $\epsilon_n^{(m-1)b}$ is in terms of equilibrium strains and $\epsilon_n^{(m-2)b}$. Continuing this process until the only non-equilibrium strain in the expression for $\epsilon_n^{(m-1)b}$ is $\epsilon_n^{-1b} \equiv 0$, we obtain the desired expression for $\epsilon_n^{(m-1)b}$. Substitution of this result into (11-b) leads to the representation

$$\epsilon_n^{(m)b} = \epsilon_{ne}^{(m)} + \sum_{j=0}^{m} \left[\epsilon_{ne}^{(j-1)} - \epsilon_{ne}^{(j)}\right] e^{-\frac{t_m - t_{j-1}}{\tau}} \tag{19}$$

where, as before, we have defined $\epsilon_{ne}^{-1} = t_{-1} = 0$. Noting that $\epsilon_m^{(m)b}$ is the strain in element (m) just when element (m) breaks, and is therefore ϵ^*,

$$\epsilon_m^{(m)b} = \epsilon^* = \epsilon_{me}^{(m)} + \sum_{j=0}^{m} \left[\epsilon_{me}^{(j-1)} - \epsilon_{me}^{(j)}\right] e^{-\frac{t_m - t_{j-1}}{\tau}} \tag{20}$$

Since all of the strains in this equation are known, as given by (10), equation (20) can be used to solve explicitly for crack tip velocity

$$v_m = \frac{\delta}{t_m - t_{m-1}} = \frac{\delta/\tau}{(t_m - t_{m-1})/\tau}$$

in which V_m is the velocity when the tip is at element (m). It will be convenient to rewrite (20) in the following form

$$\epsilon^* = \sum_{j=0}^{m} \epsilon_{me}^{(j)} \alpha_j e^{-\frac{t_m - t_j}{\tau}} \qquad m = 0, 1, 2, \cdots \tag{21}$$

where we have defined

$$\alpha_m = 1 - e^{-\frac{t_m - t_{m-1}}{\tau}}$$

To illustrate the significance of (21), it is expanded for m = 0, 1, 2, 3:

$$m=0: \quad \epsilon^* = \epsilon_{oe}^{(0)}\left[1 - e^{-\frac{t_0}{\tau}}\right] \tag{22-a}$$

$$m=1: \quad \epsilon^* = \epsilon_{1e}^{(0)}\left[1 - e^{-\frac{t_0}{\tau}}\right] e^{-\frac{t_1 - t_0}{\tau}} + \epsilon_{1e}^{(1)}\left[1 - e^{-\frac{t_1 - t_0}{\tau}}\right] \tag{22-b}$$

$$m=2: \quad \epsilon^* = \epsilon_{2e}^{(0)}\left[1 - e^{-\frac{t_0}{\tau}}\right] e^{-\frac{t_2 - t_0}{\tau}} + \epsilon_{2e}^{(1)}\left[1 - e^{-\frac{t_1 - t_0}{\tau}}\right] e^{-\frac{t_2 - t_1}{\tau}} + \epsilon_{2e}^{(2)}\left[1 - e^{-\frac{t_2 - t_1}{\tau}}\right] \tag{22-c}$$

$$m=3: \quad \epsilon^* = \epsilon_{3e}^{(0)}\left[1 - e^{-\frac{t_0}{\tau}}\right] e^{-\frac{t_3 - t_0}{\tau}} + \epsilon_{3e}^{(1)}\left[1 - e^{-\frac{t_1 - t_0}{\tau}}\right] e^{-\frac{t_3 - t_1}{\tau}} + \epsilon_{3e}^{(2)}\left[1 - e^{-\frac{t_2 - t_1}{\tau}}\right] e^{-\frac{t_3 - t_2}{\tau}} + \epsilon_{3e}^{(3)}\left[1 - e^{-\frac{t_3 - t_2}{\tau}}\right] \tag{22-d}$$

It is clear that if $\frac{t_m - t_0}{\tau} \ll 1$, the exponential terms which multiply α_m can be taken as unity so that (21) becomes

$$\epsilon^* \doteq \sum_{j=0}^{m} \epsilon_{me}^{(j)} \alpha_j \tag{23}$$

Utilizing (22-a) for ϵ^*, we can rewrite (23) as

$$\frac{w_m}{w_o} = 1 - \sum_{j=o}^{m-1} \frac{\epsilon_{me}^{(j)}}{\epsilon_{je}^{(j)}} \frac{w_j}{w_o} \tag{24}$$

where

$$\frac{w_m}{w_o} = \frac{\epsilon_{me}^{(m)}}{\epsilon_{oe}^{(o)}} \frac{\alpha_m}{\alpha_o}$$

If it is further assumed that only the first term in the equilibrium strain (10) need be considered (i.e., that the strain resulting from the leading term in the stresses (1-b) and (2-b) provides the main contribution to failure) then from (10)

$$\epsilon_{me}^{(j)} \cong \frac{\sigma_o}{E_v \sqrt{\frac{2\delta}{b+j\delta}}} \left[(m-j+1)^{\frac{1}{2}} - (m-j)^{\frac{1}{2}} \right] \tag{25-a}$$

and

$$\epsilon_{me}^{(m)} \cong \frac{\sigma_o}{E_v \sqrt{\frac{2\delta}{b+m\delta}}} \tag{25-b}$$

Substituting (25) into (24) gives the recurrence expression for $\frac{w_m}{w_o}$:

$$\frac{w_m}{w_o} = 1 - \sum_{j=o}^{m-1} \left[(m-j+1)^{\frac{1}{2}} - (m-j)^{\frac{1}{2}} \right] \frac{w_j}{w_o} \tag{26}$$

Calculations give, for example

$$\frac{w_o}{w_m} = 1,\ 1.71,\ 2.27,\ 2.75,\ \cdots \quad \text{for} \quad m = 0, 1, 2, 3, \cdots$$

It can be deduced that

$$\frac{w_m}{w_o} \cong \frac{2}{\pi\sqrt{m}} \qquad \text{for} \quad m \geq 4 \tag{27}$$

Under the assumption that $\frac{t_m}{\tau} \ll 1$,

$$\alpha_m \cong \frac{t_m - t_{m-1}}{\tau}$$

so that

$$\frac{w_m}{w_o} = \frac{\epsilon_{me}^{(m)} \alpha_m}{\epsilon_{oe}^{(o)} \alpha_o} \cong \frac{\sigma_o \sqrt{b} \sqrt{1 + m\delta/b}}{E_v \epsilon^* \sqrt{2}\sqrt{\delta}} \frac{t_m - t_{m-1}}{\tau}$$

$$= \frac{\sigma_o \sqrt{1 + m\delta/b}}{E_v \epsilon^* \sqrt{2}} \frac{\sqrt{\delta b}}{2 v_m} \tag{28}$$

Solving for V_m and using (27) we find

$$v_m \cong \frac{\pi}{2\sqrt{2}} \frac{\sigma_0/E_V}{\epsilon^*} \frac{b}{2} \sqrt{\frac{m\delta}{b}\left(1+\frac{m\delta}{b}\right)} \qquad m \geq 4 \tag{29}$$

showing that the velocity increases without bound is the crack grows which is impossible because free running cracks are known to be limited by speeds of the order of half the shear wave speed. However such a result is not surprising since inertia has not been included in the formulation. Nevertheless (29) may provide a reasonable approximation to the crack tip speed if it is sufficiently less than the shear wave speed.

Passing to the continuous form by letting $m\delta = s$, in which s is the distance the crack tip has traveled, we have

$$v = \frac{ds}{dt} \cong \frac{\pi}{2\sqrt{2}} \frac{\sigma_0/E_V}{\epsilon^*} \frac{b}{2} \sqrt{\frac{s}{b}\left(1+\frac{s}{b}\right)} \qquad s \geq 4\delta \tag{30-a}$$

which shows

$$v \propto \sqrt{\frac{s}{b}} \qquad \frac{4\delta}{b} \leq \frac{s}{b} \ll 1 \tag{30-b}$$

$$v \propto \frac{s}{b} \qquad \frac{s}{b} \gg 1 \tag{30-c}$$

The initial behavior indicated in (30-b) results from the increasing amount of strain which accumulates in the elements ahead of the crack as it propagates. This increase in velocity when $s \ll b$ occurs while the stress at the crack tips remain essentially constant as seen from equation (4-b) However, the fact that the stress is proportional to $\sqrt{s}$ for $s \gg 1$ accounts for the more rapid increase in velocity shown by (30-c).

The time dependence of crack growth can be determined from (30-a) by integration:

$$\sqrt{1+\frac{s}{b}} + \sqrt{\frac{s}{b}} \cong e^{\frac{\pi}{4\sqrt{2}} \frac{\sigma_0/E_V}{\epsilon^*} \frac{t}{2}} \tag{31-a}$$

so that

$$\frac{s}{b} \cong \left[\frac{\pi}{4\sqrt{2}} \frac{\sigma_0/E_V}{\epsilon^*} \frac{t}{2}\right]^2 \qquad \frac{4\delta}{b} \leq \frac{s}{b} \ll 1 \tag{31-b}$$

$$\frac{s}{b} \cong \frac{1}{4} e^{\frac{\pi}{2\sqrt{2}} \frac{\sigma_0/E_V}{\epsilon^*} \frac{t}{2}} \qquad \frac{s}{b} \gg 1 \tag{31-c}$$

Remarks. -

The proposed phenomenological model is by no means unique, with it being possible to include a more complicated material representation instead of the incompressible VOigt model used here. Also it should be possible to introduce a more sophisticated fracture criterion if necessary, based not upon maximum strain, but perhaps octahedral strain as a function of strain rate and cumulative damage. Further, for ease in manipulation, the discrete element formulation might be replaced by a continuous material formulation. Finally a basic investigation might be conducted to ascertain the physical significance of the characteristic strand diameter, δ , incorporated in the analysis.

APPENDIX 5.3 - Large Plane Strain Analysis for Distortion Energy in a Hollow Tube

The strain transformation in cylindrical coordinates is given by

$$\bar{r} = \bar{r}(r) \; ; \quad \bar{\theta} = \theta \; ; \quad \bar{z} = z \tag{1}$$

Here the superscript bar indicates the deformed or Eulerian coordinate. The Jacobian of the transformation is given by

$$\begin{vmatrix} d\bar{r} \\ \bar{r}\,d\bar{\theta} \\ d\bar{z} \end{vmatrix} = \begin{vmatrix} \frac{d\bar{r}}{dr} & 0 & 0 \\ 0 & \frac{\bar{r}}{r} & 0 \\ 0 & 0 & 1 \end{vmatrix} \begin{vmatrix} dr \\ r\,d\theta \\ dz \end{vmatrix} \tag{2}$$

Incompressibility demands that

$$\frac{d\bar{r}}{dr} \times \frac{\bar{r}}{r} \times 1 = 1 \tag{3}$$

$$\bar{r}^2 = r^2 + \bar{a}^2 - a^2 = \lambda^2 r^2 \tag{4}$$

$$\lambda^2 = 1 + \frac{\bar{a}^2 - a^2}{r^2} \tag{5}$$

$$\frac{d\bar{r}}{dr} = \frac{1}{\lambda}$$

Substitution into (2) yields

$$\frac{\bar{\sigma}_r}{\mu} = \frac{1}{\lambda^2} + \bar{k} \tag{6}$$

$$\frac{\bar{\sigma}_\theta}{\mu} = \lambda^2 + \bar{k} \tag{7}$$

The equilibrium equation is cast in Eulerian coordinates

$$\frac{\bar{\sigma}_\theta - \bar{\sigma}_r}{\bar{r}} = \frac{d\bar{\sigma}_r}{d\bar{r}} \tag{8}$$

Substituting (6) and (7) yields after integration

$$\bar{k} = c - \ln\lambda - \frac{1}{2\lambda^2} \tag{9}$$

$$\frac{\bar{\sigma}_r}{\mu} = c - \ln\lambda + \frac{1}{2\lambda^2} \tag{10}$$

At the inner surface, radius a

$$\lambda_a = \frac{\bar{a}}{a} \tag{11}$$

$$-\frac{p}{\mu} = c - \ln\lambda_a + \frac{1}{2\lambda_a^2} \tag{12}$$

At the propellant-case interface, the radial stress (r=b) is taken to be $-P_i$

$$-\frac{p_i}{\mu} = c - \ln\lambda_b + \frac{1}{2\lambda_b^2} \tag{13}$$

$$\lambda_b^2 = 1 + m(\lambda_a^2 - 1) \tag{14}$$

where again

$$m = \frac{a^2}{b^2} \tag{15}$$

$$\frac{p - p_i}{\mu} = \frac{1}{2\lambda_b^2} - \frac{1}{2\lambda_a^2} + \ln\frac{\lambda_a}{\lambda_b} \tag{16}$$

The strain energy is easily seen to be a maximum at a , so that

$$W_a = \frac{\mu}{2}\left(I_{1a} - 3\right) = \frac{\mu}{2}\left(\lambda_a^2 + \frac{1}{\lambda_a^2} - 2\right) \tag{17}$$

The interfacial pressure is determined by matching with the case. We have using a prime to indicate properties in the metal

$$\sigma_r = A - \frac{B}{r^2} \tag{18}$$

$$\frac{u}{r} = A\,\frac{1-2\nu'}{2\mu'} + \frac{1}{r^2}\,\frac{B}{2\mu'} \tag{19}$$

At r=b, we have

$$-p_i = A - \frac{B}{b^2} \tag{20}$$

$$\frac{\lambda_b^2 - 1}{2} = \left(\frac{u}{r}\right)_b = \frac{A(1-2\nu')}{2\mu'} + \frac{B}{2\mu' b^2} \tag{21}$$

Note that we equate $(u/r)_b$ to the finite (Murnaghan strain) to be consistent with large strain theory, even though we use small strain theory in the case. At the outer surface of the case, the pressure is assumed to be zero, so that

$$B = Ac^2 \tag{22}$$

Solution is expedited by defining, as before

$$\phi = \frac{\mu}{\mu'}\left(1 + \frac{2-2\nu'}{\delta}\right) \tag{23}$$

so that

$$\lambda_b^2 - 1 = \frac{p_i}{\mu}\,\phi \tag{24}$$

Substitution into (6) yields

$$\frac{p}{\mu} = \frac{1}{2\lambda_b^2} - \frac{1}{2\lambda_a^2} + \ln\frac{\lambda_a}{\lambda_b} + \frac{\lambda_b^2 - 1}{\phi} \tag{25}$$

and with (64), there results

$$\frac{2p}{\mu} = \frac{1}{1+m(\lambda_a^2-1)} - \frac{1}{\lambda_a^2} + \ln\frac{\lambda_a^2}{1+m(\lambda_a^2-1)} + \frac{2}{\phi}m(\lambda_a^2-1) \tag{26}$$

Since λ_a will be approximately 4 near the yield, (6) is easily approximated by

$$\frac{p}{\mu} = \frac{m}{\phi}(\lambda_a^2 - 1) \qquad \text{using } m = a/b \tag{27}$$

and the strain energy becomes

$$W = \frac{p^2\phi^2}{2mp\phi + 2\mu m^2} \tag{28}$$

This expression is to be compared with (8) for $\nu = \frac{1}{2}$

$$W_{max} = \frac{3p^2\phi^2}{2\mu[\phi + m(1-\phi)]^2} \approx \frac{3p^2\phi^2}{2\mu m^2} \tag{29}$$

for small ϕ. Thus, in small strain theory, the energy increases quadratically with pressure, whereas the dependence becomes linear in the large strain theory, i.e.,

$$W \approx \frac{p\phi}{2m} \tag{30}$$

FIGURES

Fig. 1 - Stress-strain curve in simple tension at room temperature for natural rubber vulcanizate.

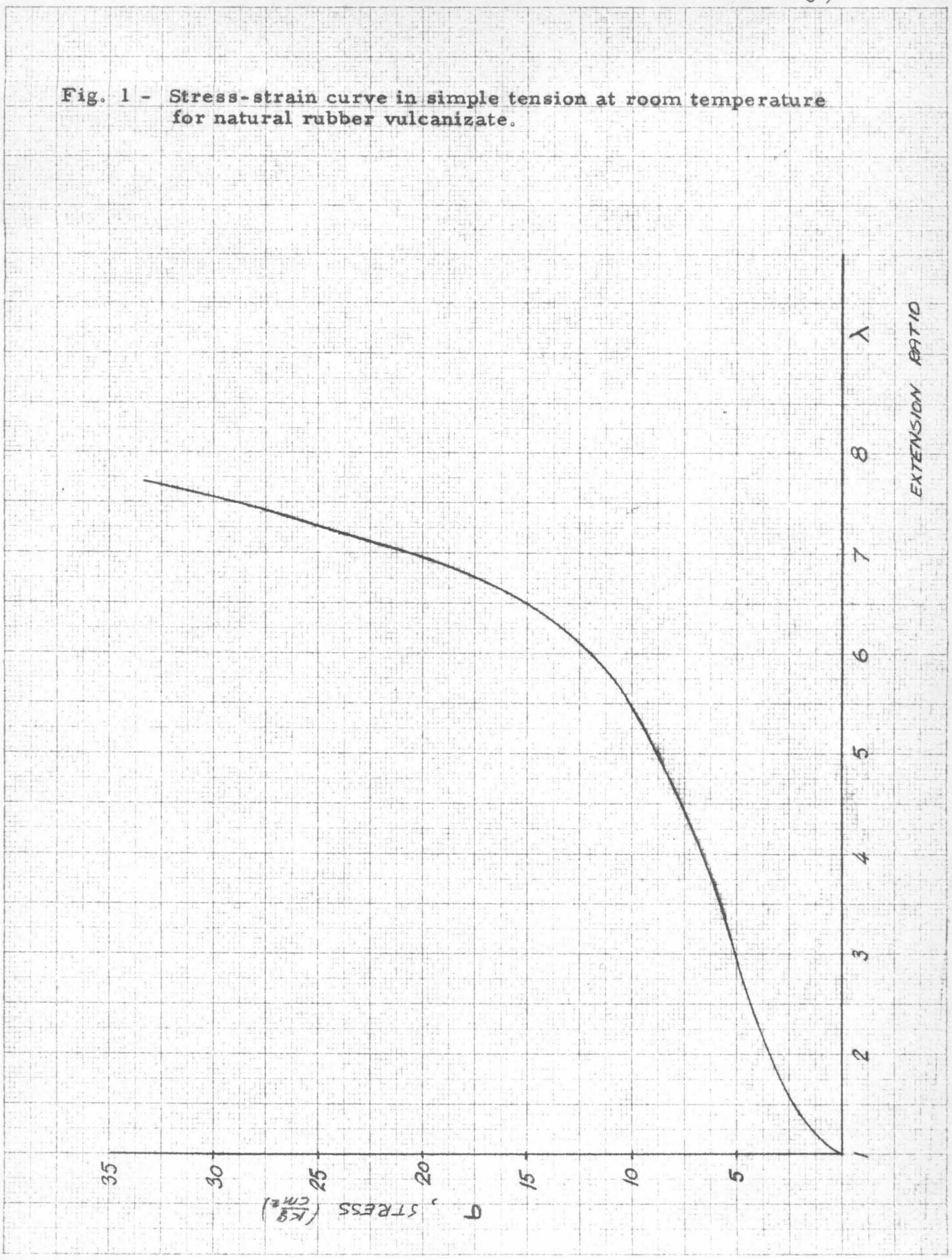

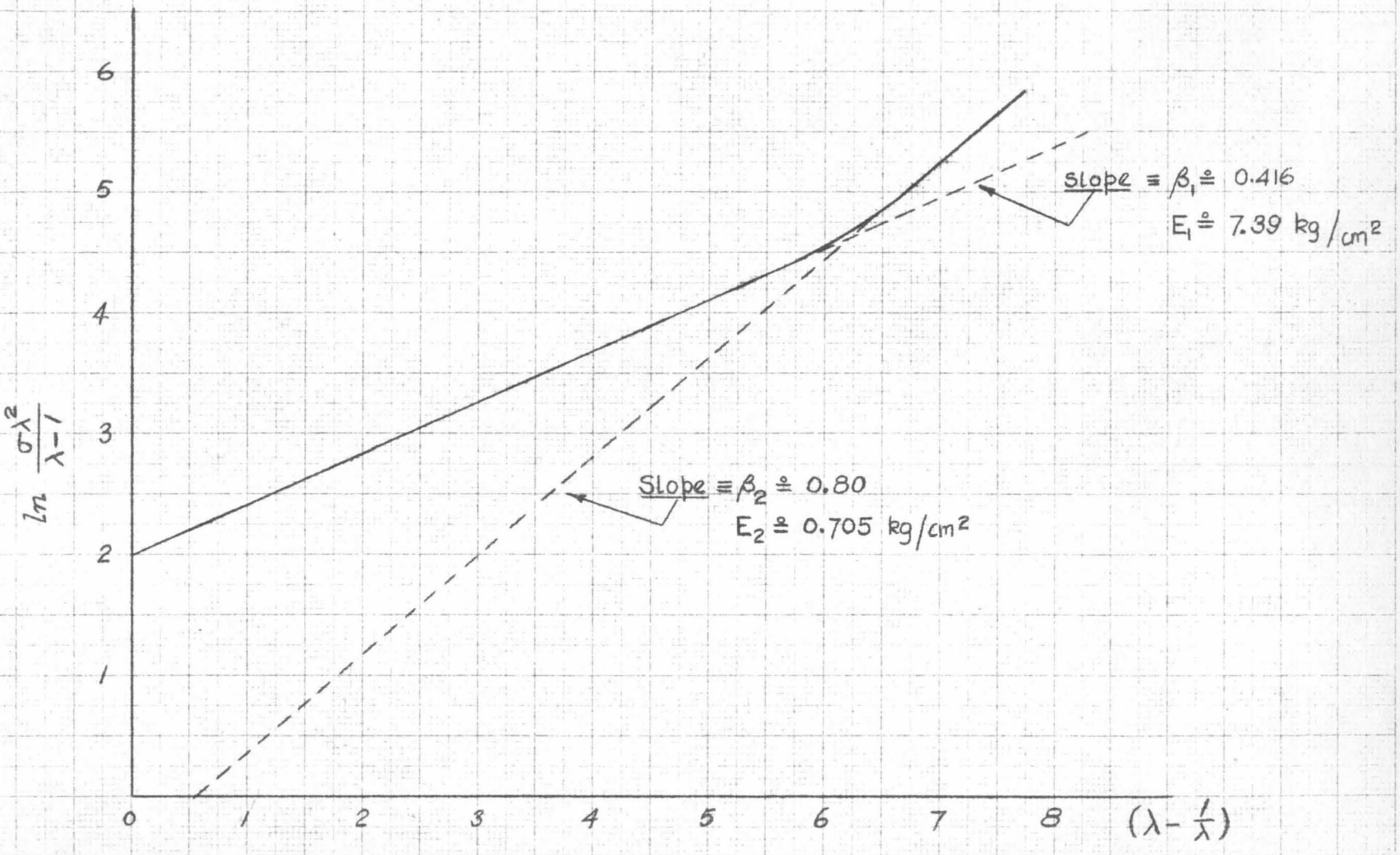

Fig. 2 - Rectified stress-strain curve from Roth, Metz, Stiehler correlation (Reference 12).

Fig. 3 - Distortion strain energy as a function of extension ratio for natural rubber vulcanizate.

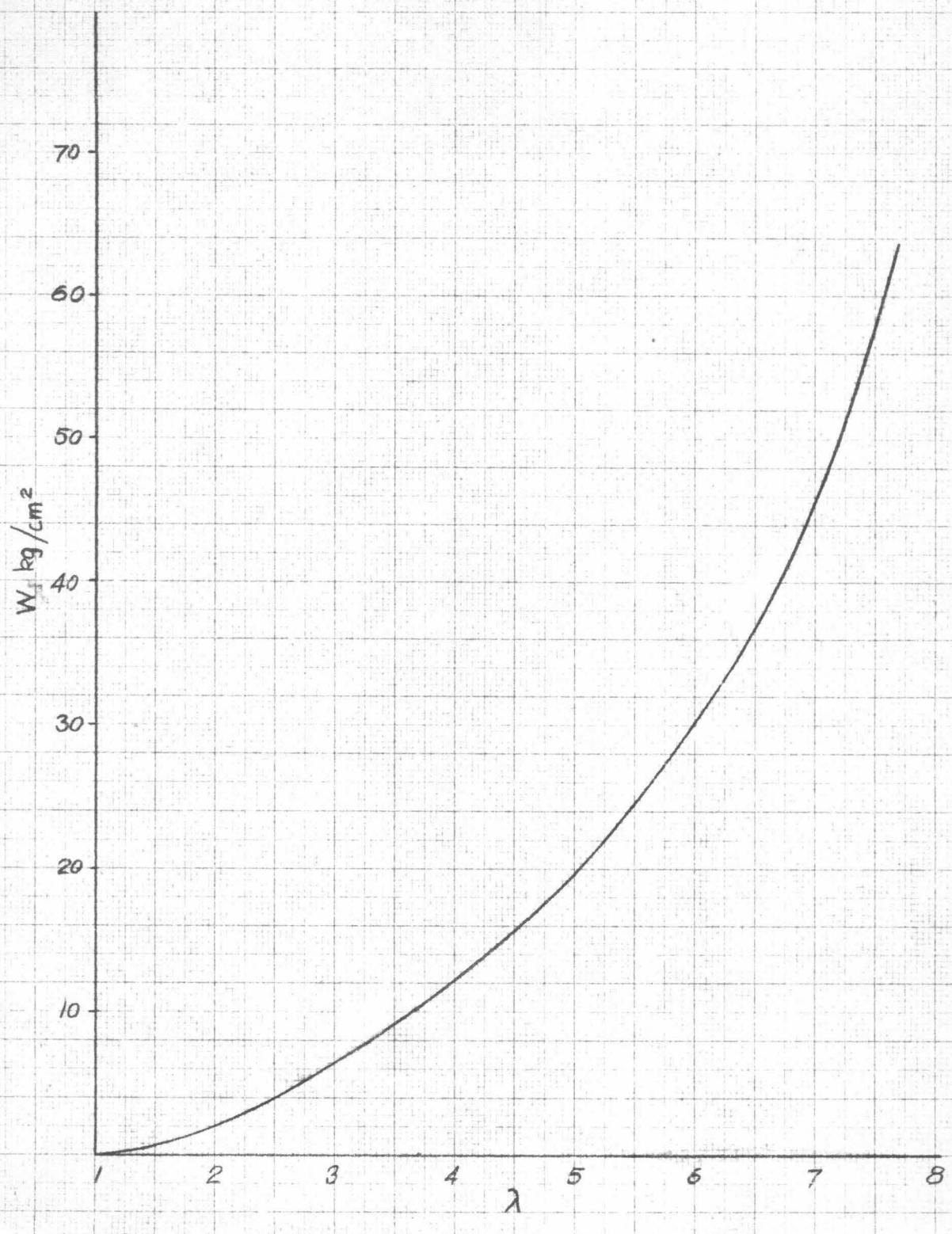

Fig. 4 - Correlation between measured distortion strain energy and the theoretical function predicted by network theory.

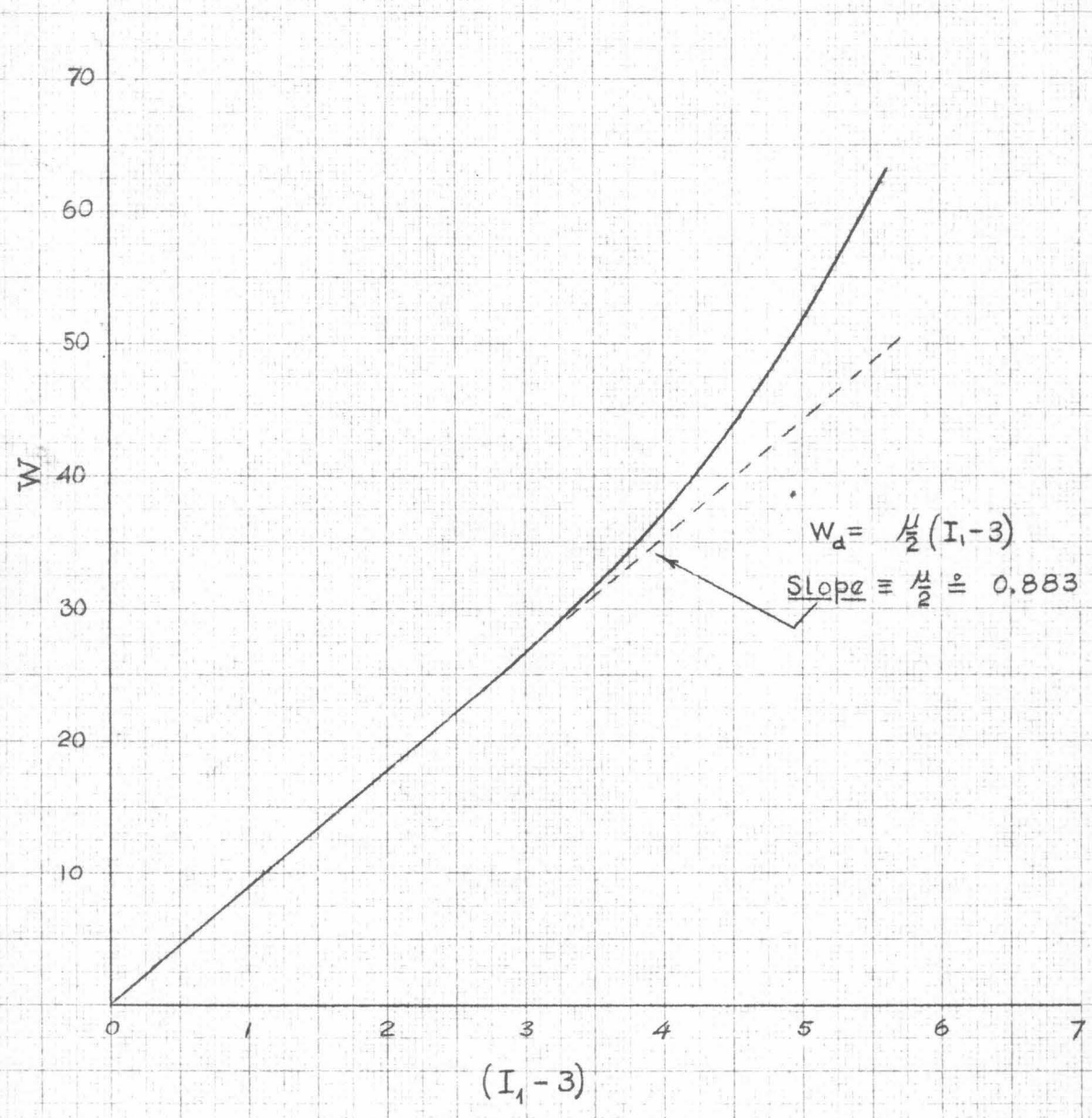

Fig. 5 - Relation between distortion strain energy and the second strain invariant.

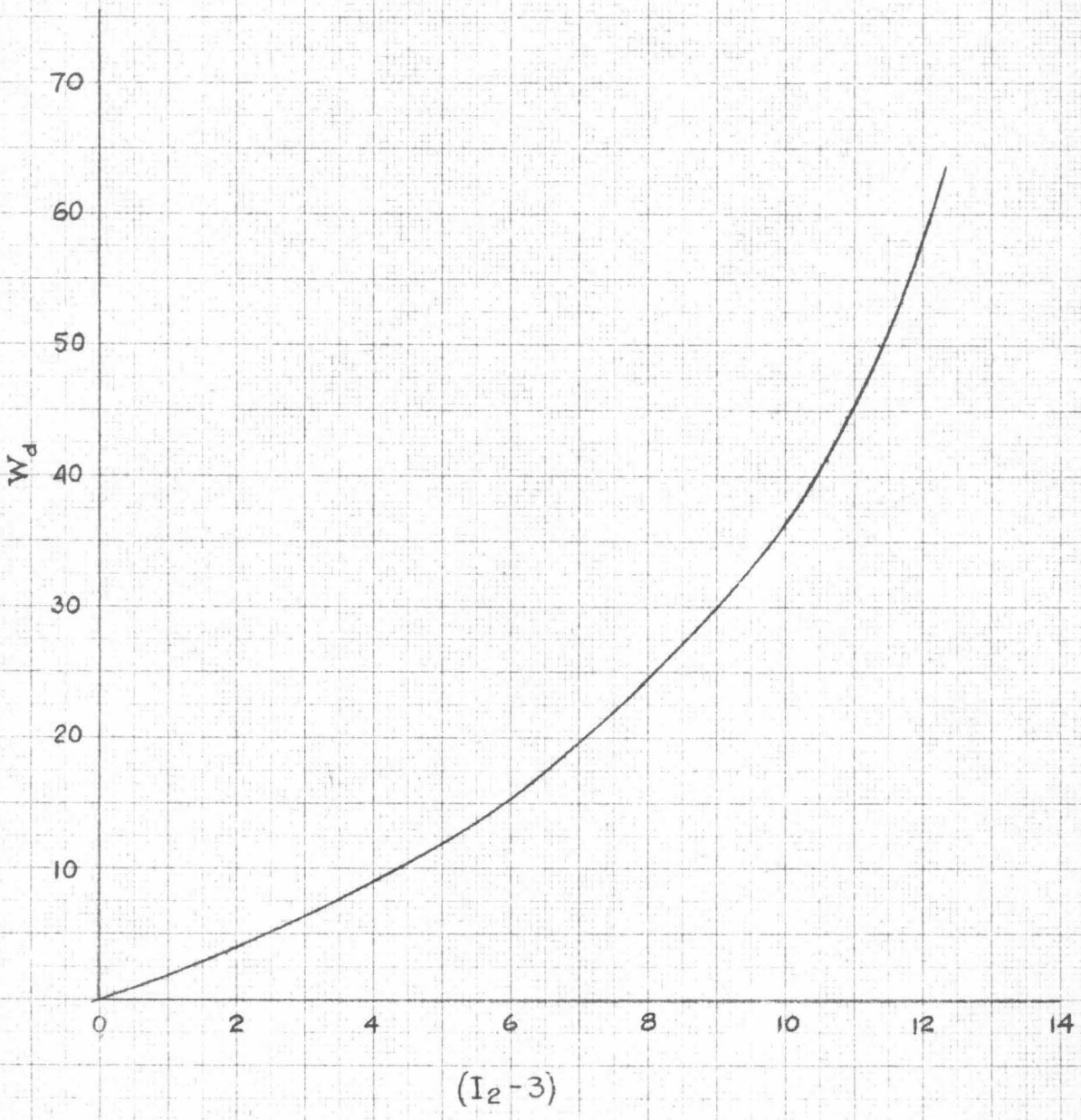

Fig. 6 - Poisson's Ratio vs finite strain.

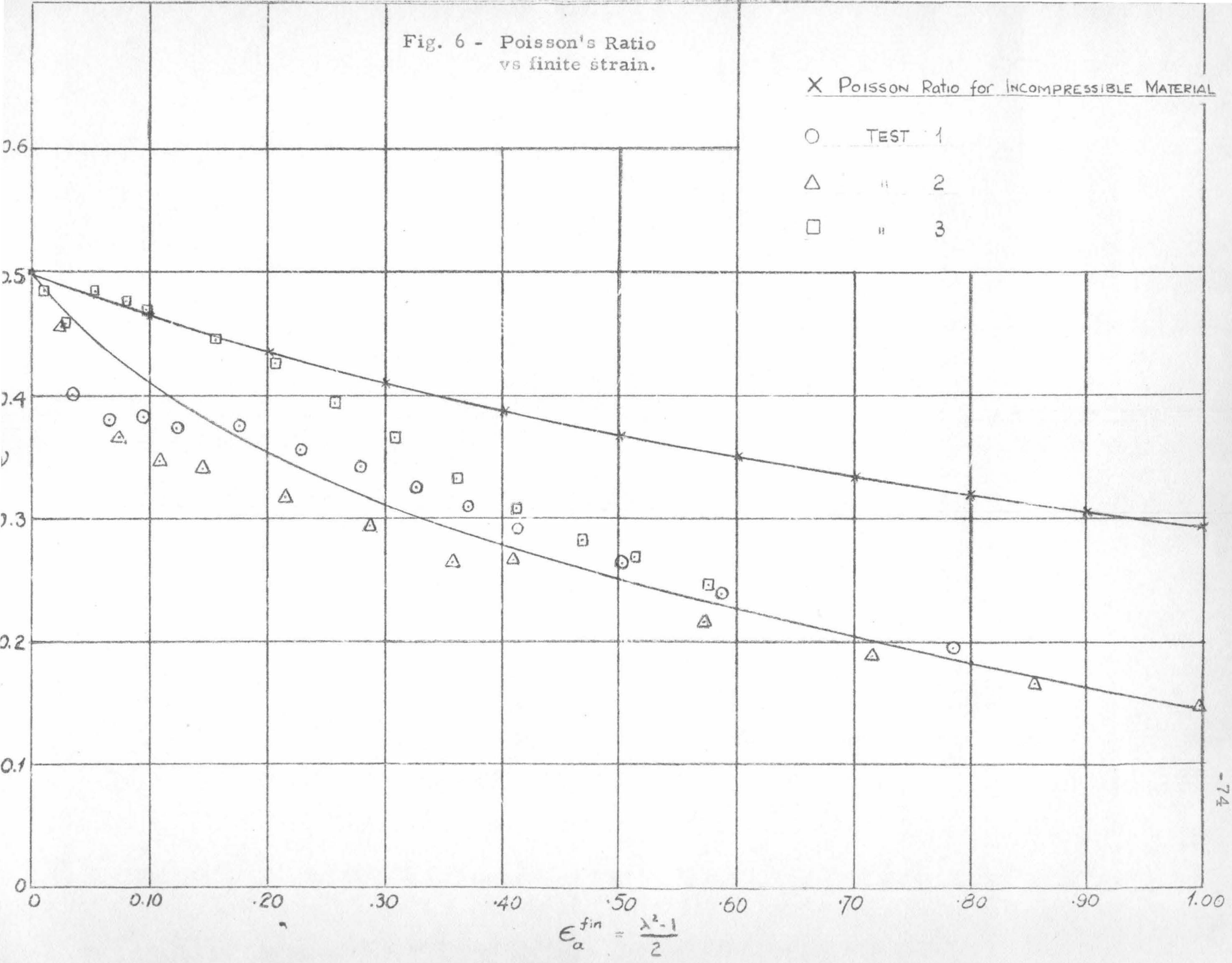

Fig. 7 - Simple compressive-tensile behavior of polyurethane propellant at room temperature.

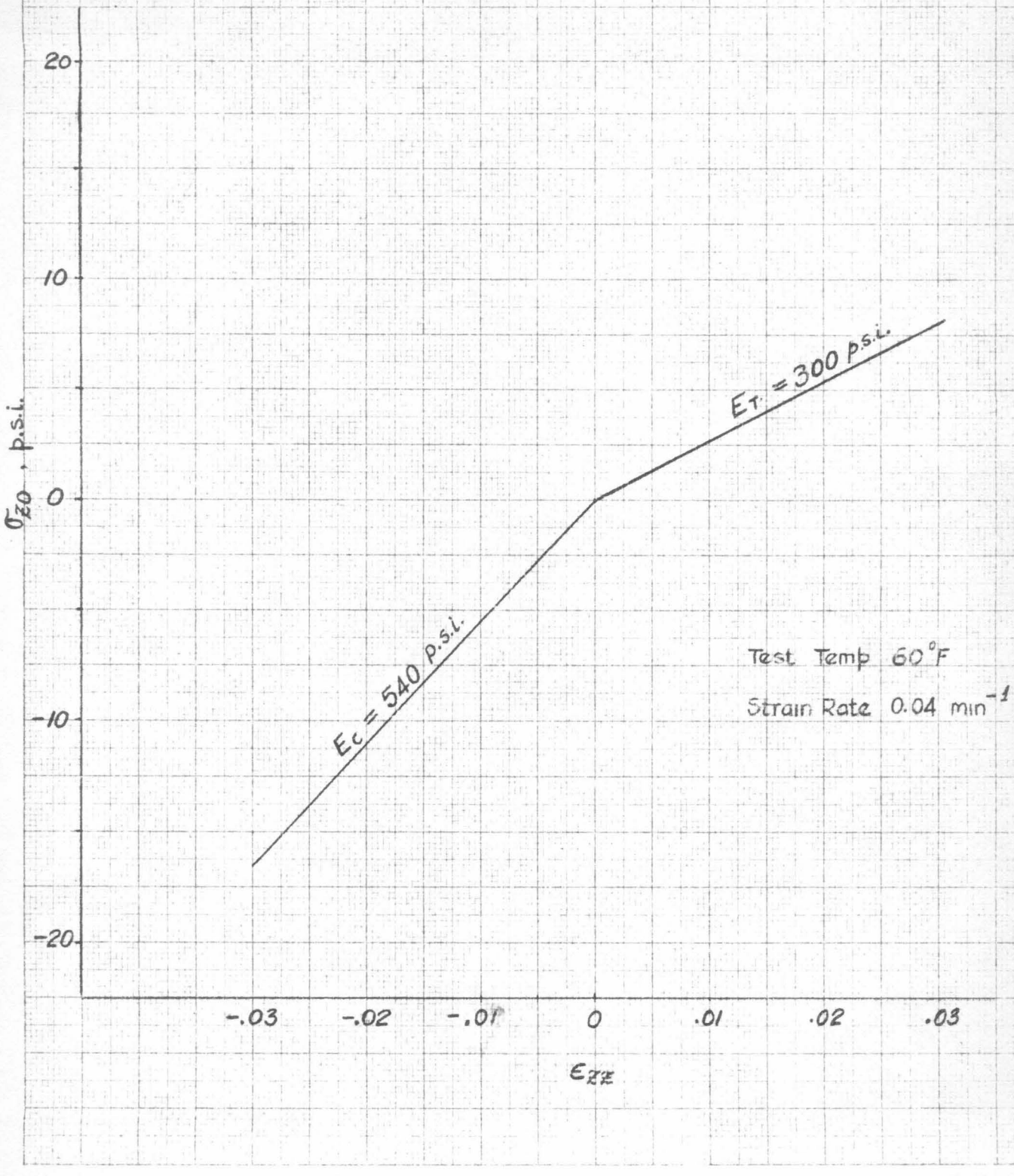

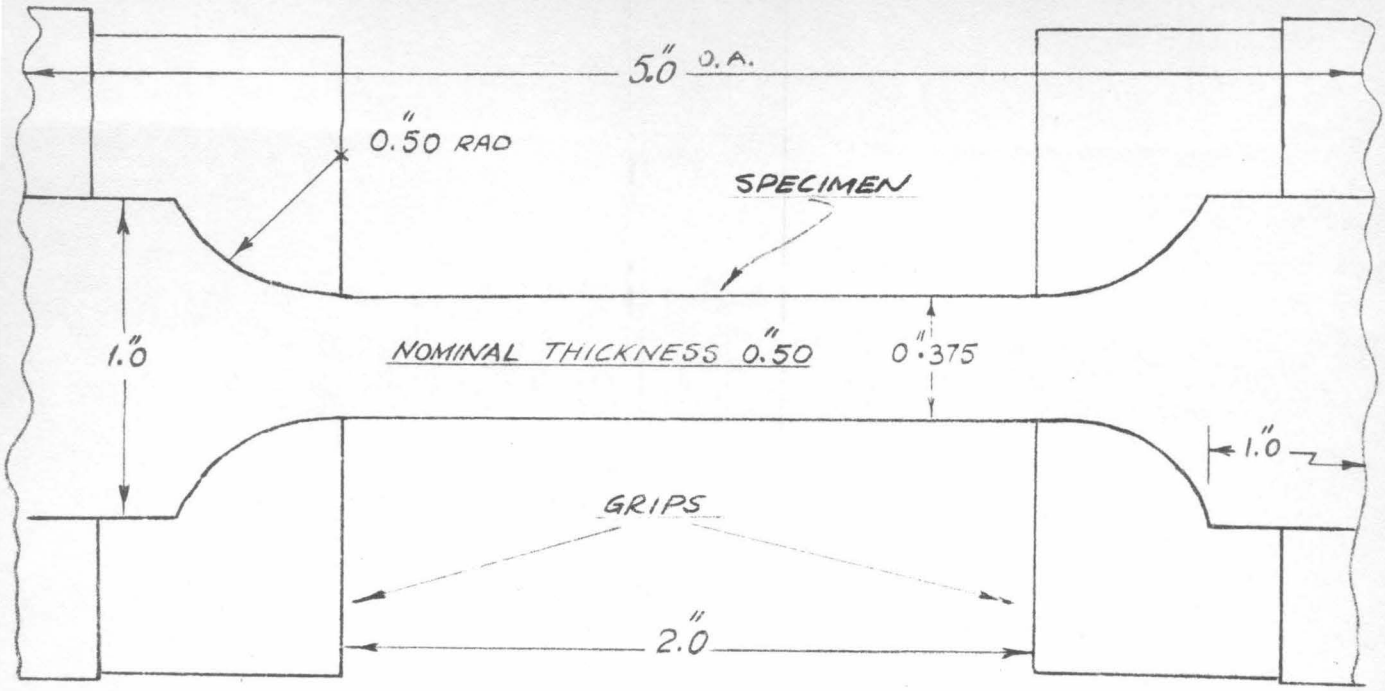

Fig. 8 - Standard JANAF tensile specimen.

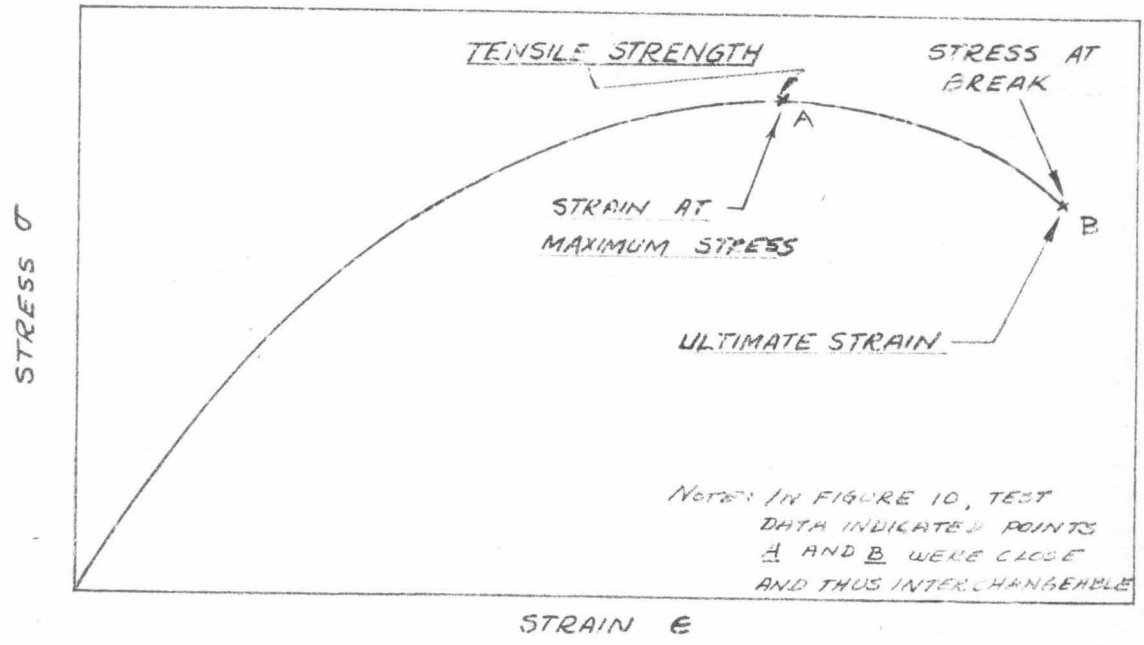

Fig. 9 - Typical Instron tensile curve.

Fig. 10 - Ultimate strain master curve (Landel and Smith, Jet Propulsion Laboratory, External Publication No. 655, June 1959).

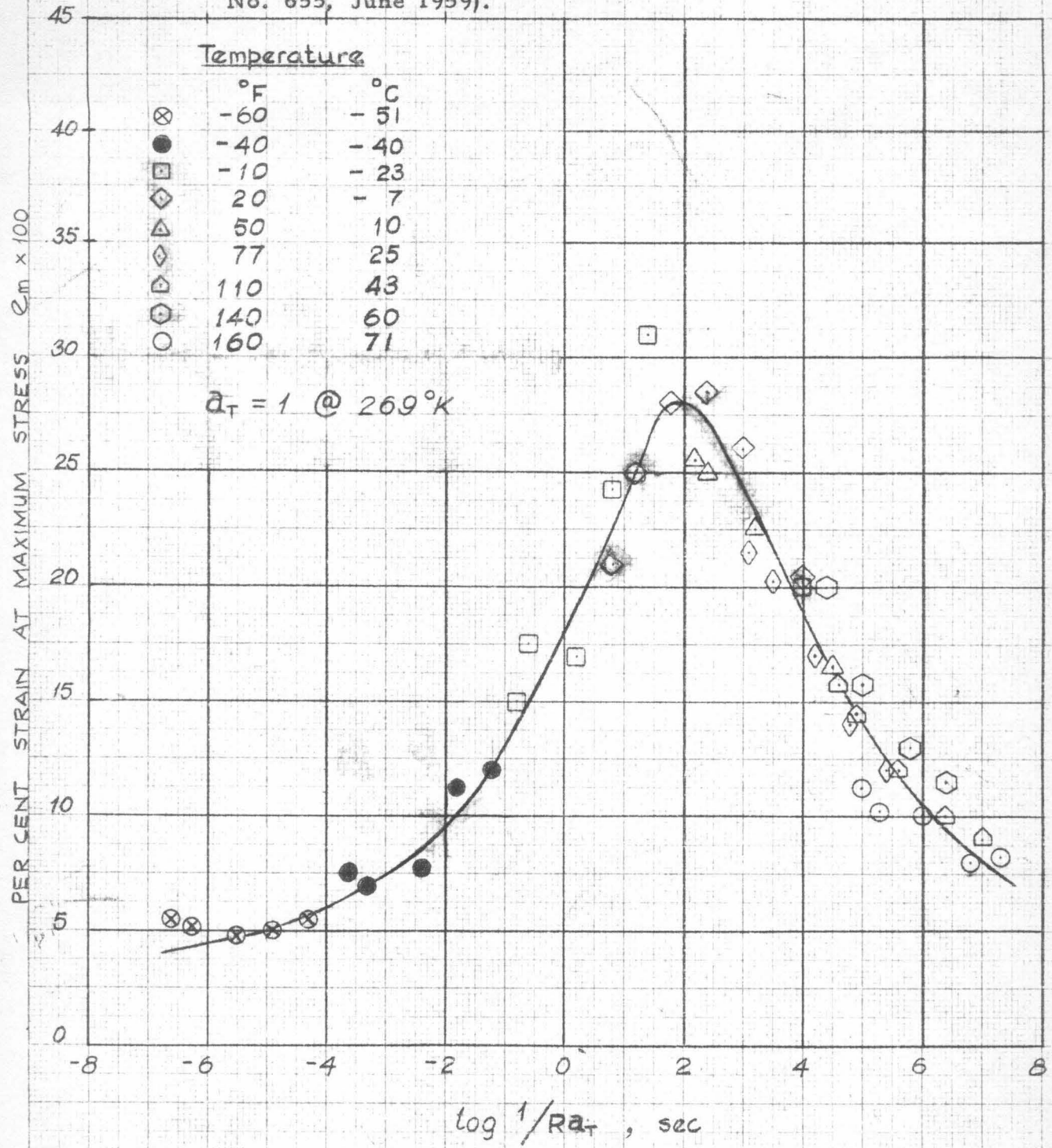

Fig. 11 - Ultimate stress master curve (Landel and Smith, Jet Propulsion Laboratory, External Publication No. 655, June 1959).

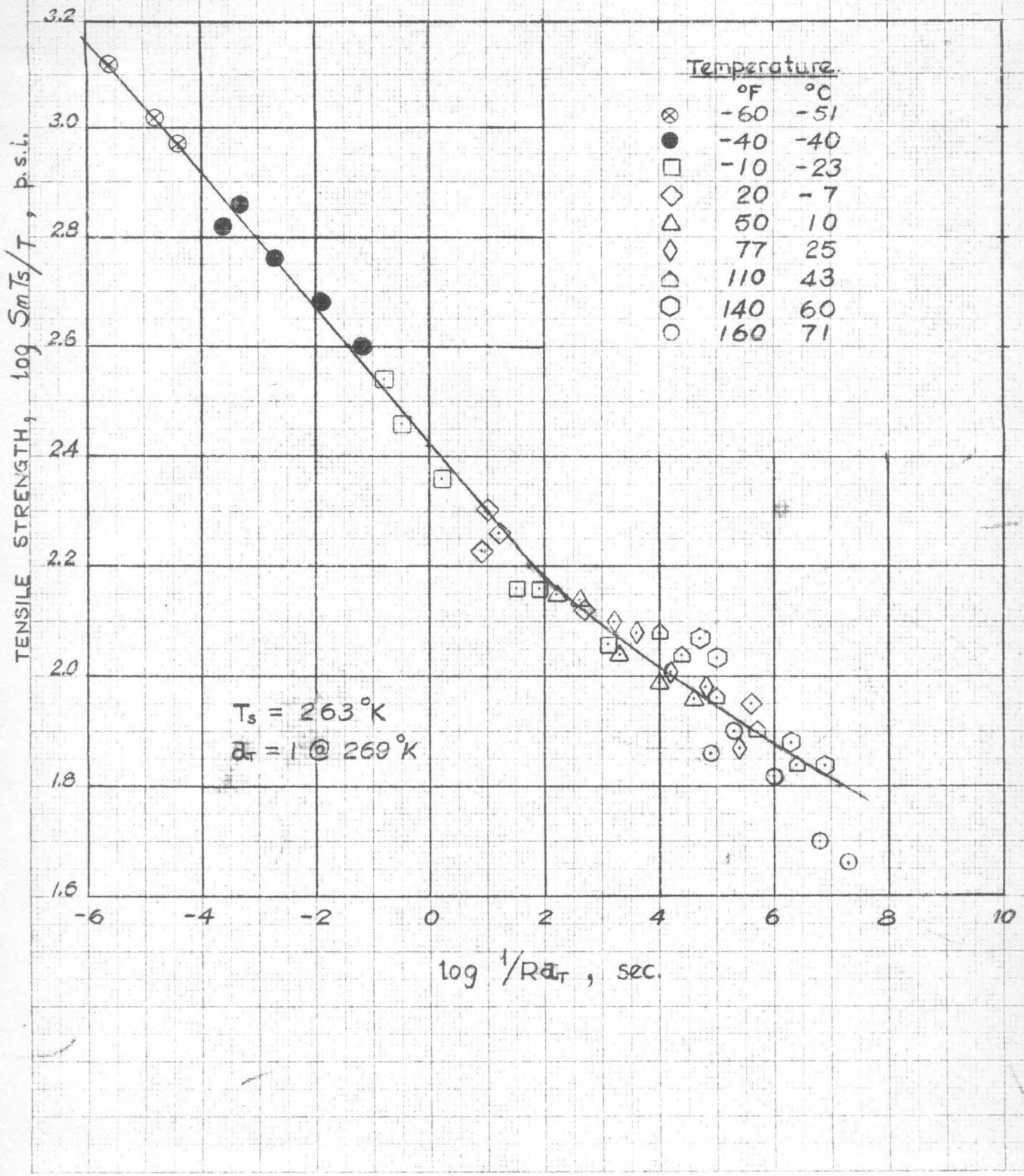

Fig. 12 - Triaxial fracture data (Reference 20), for various compositions

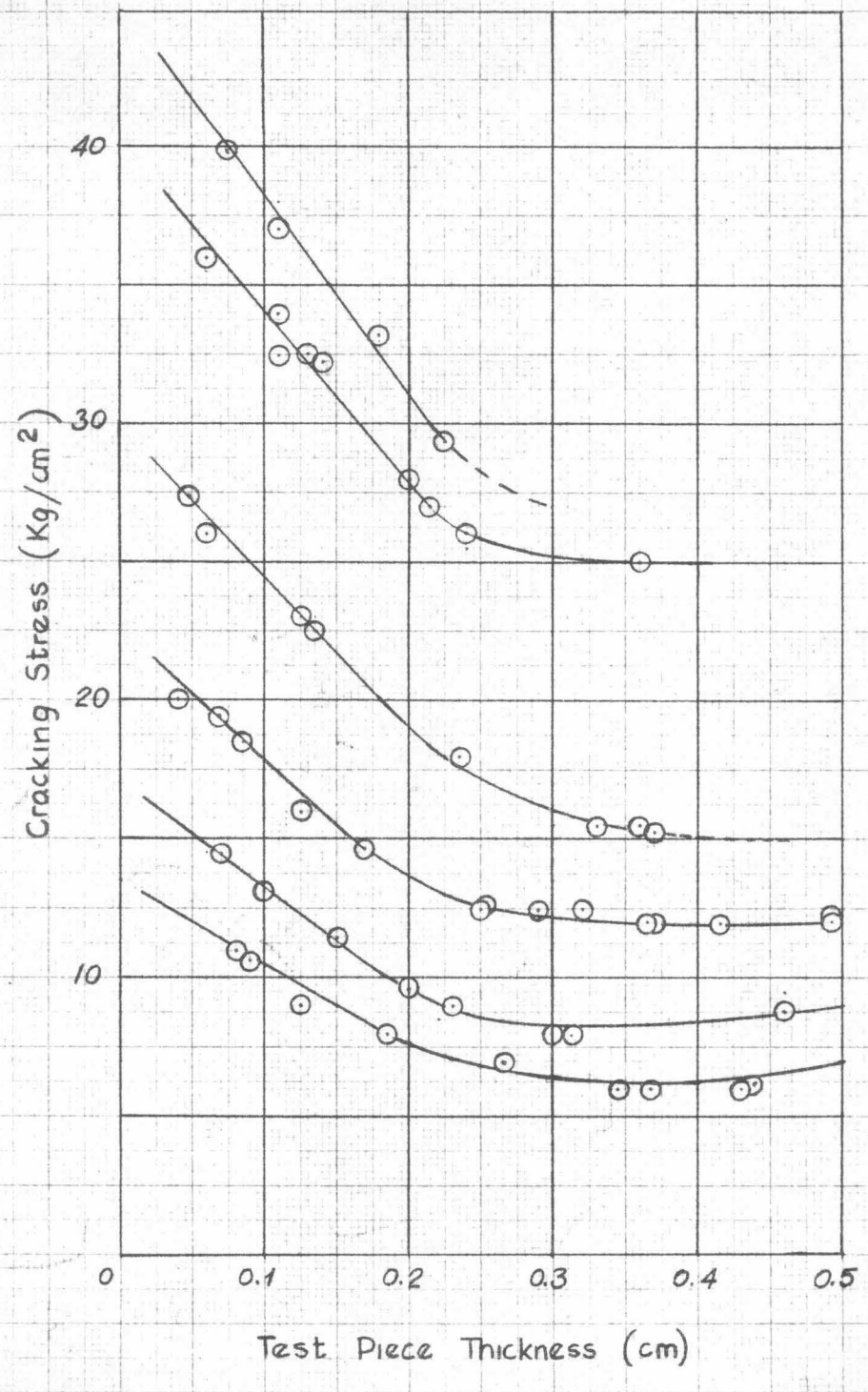

Fig. 13 - Axial elongation as a function of torsional shear.

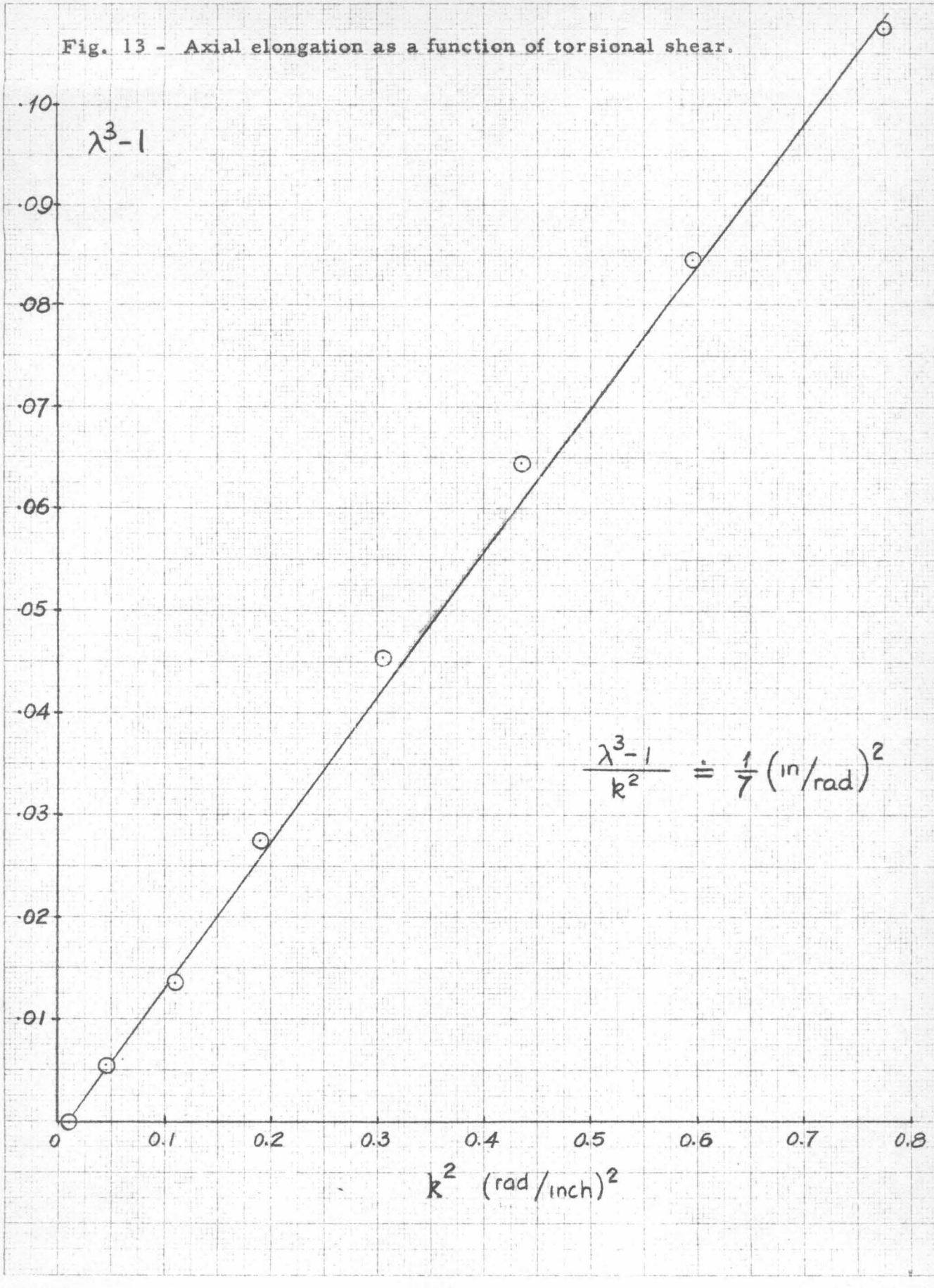

Fig. 14 - Maximum gross area stress before self-propagation of crack as a function of crack length at that stress level. (Paper No. 57-SA-12, J. Frisch, presented at semi-annual meeting, ASME, San Francisco)

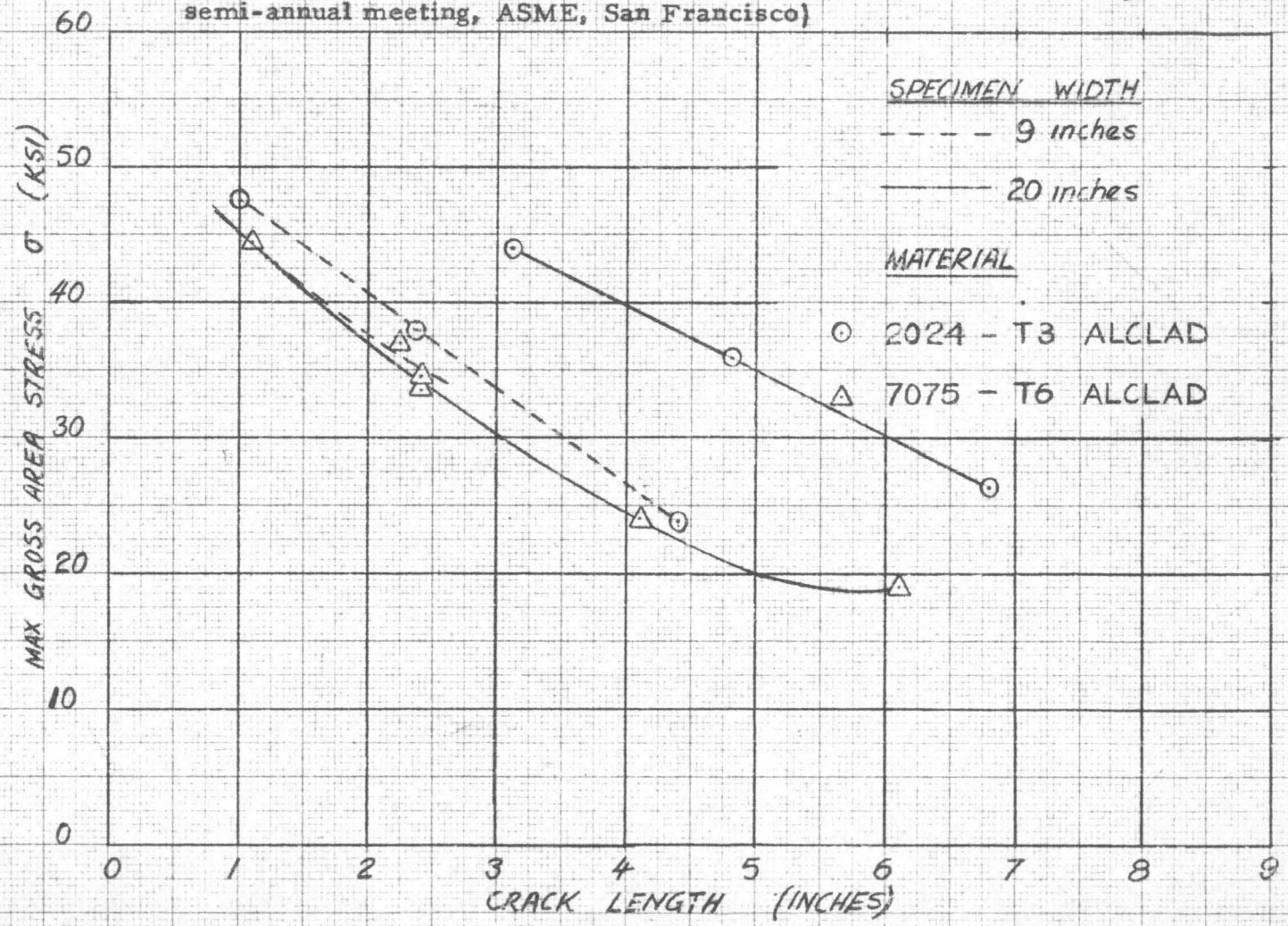

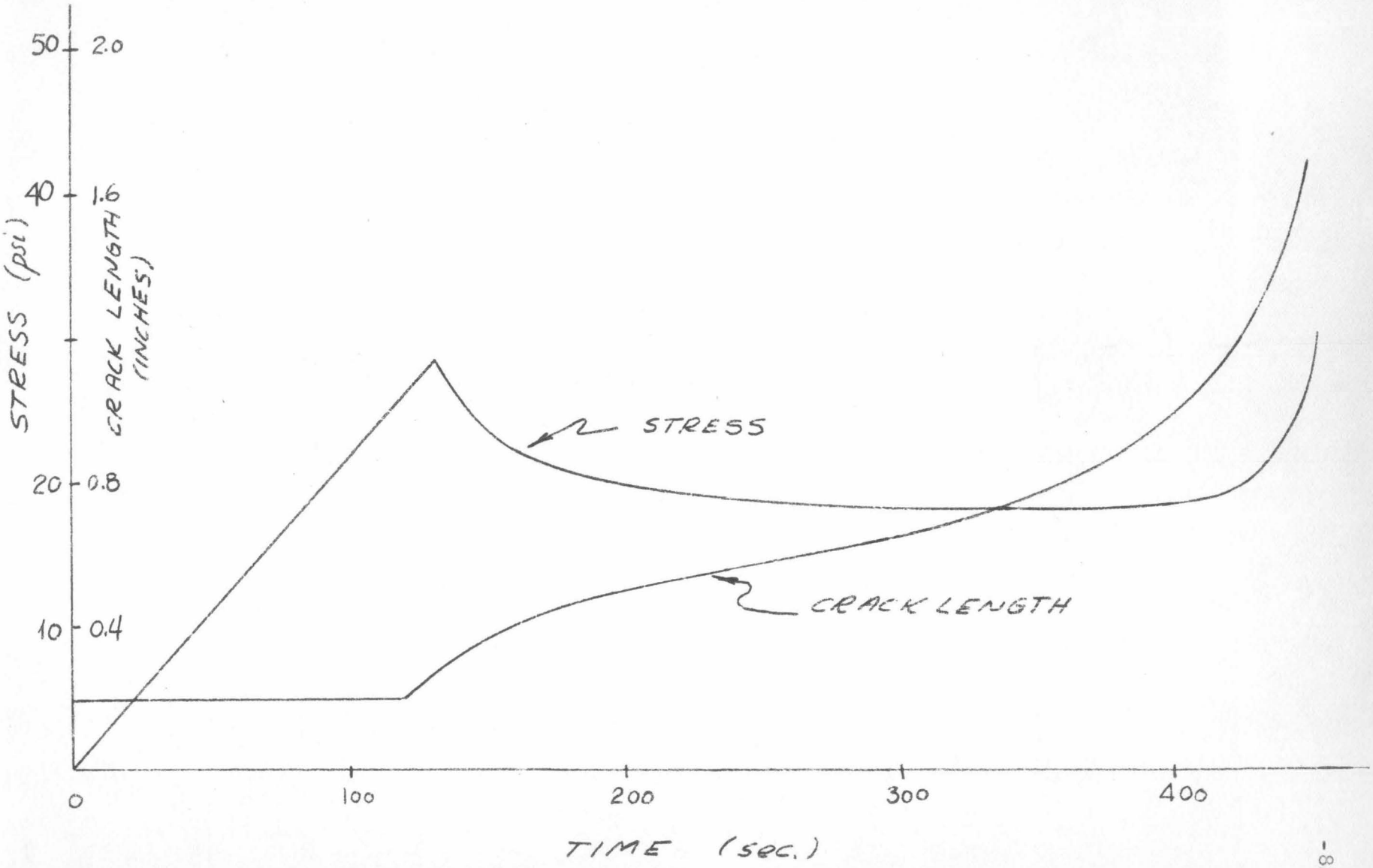

Fig. 15 - Typical data for crack growth in simulated propellant material (Reference 25).

Fig. 16 - Maximum strain energy density vs Poisson's ratio.

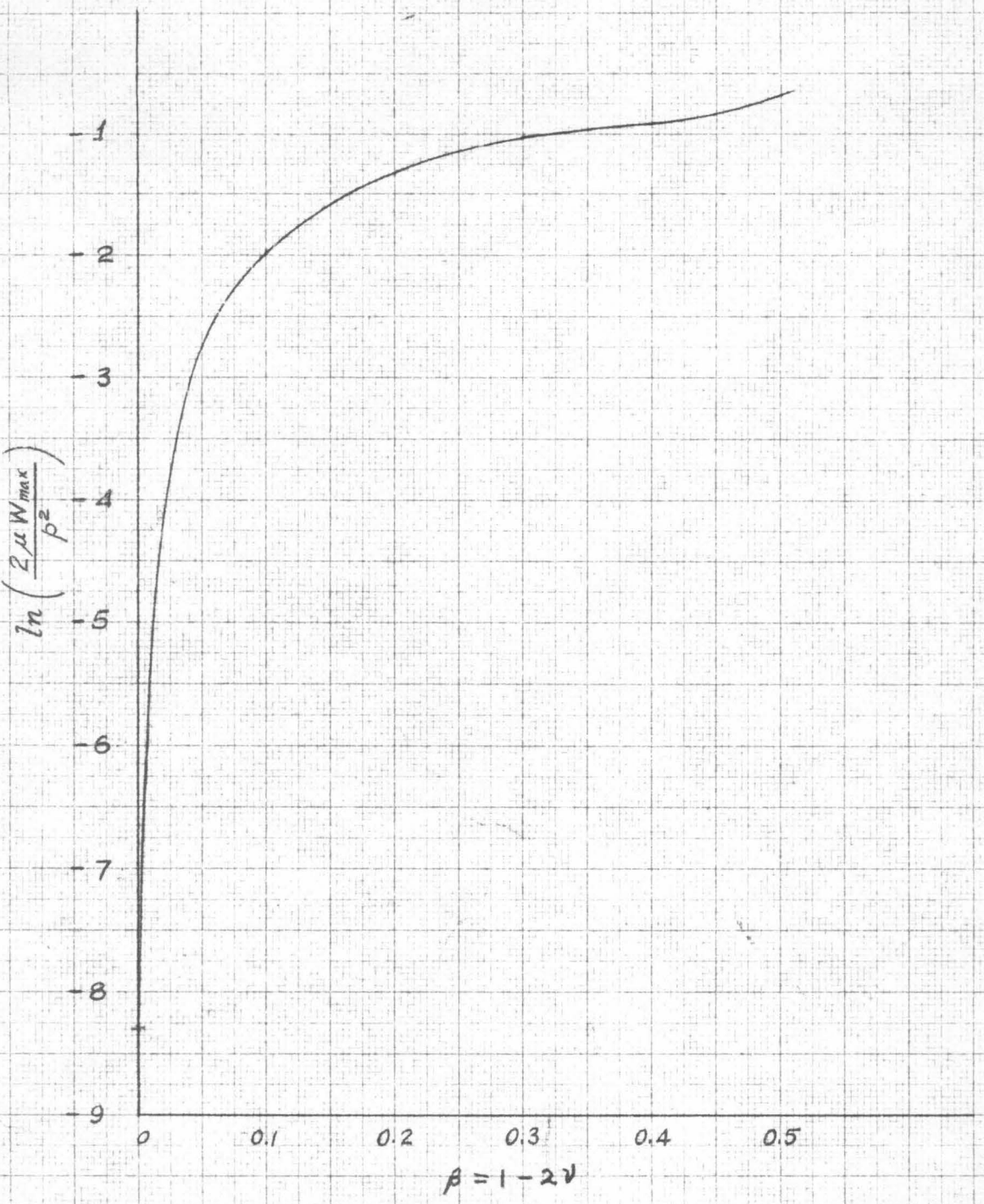

REFERENCES

1. Schapery, R. A., Stimpson, L. E., and Williams, M. L.: "Fundamental Studies Relating to Systems Analysis of Solid Propellants", California Institute of Technology GALCIT 101, Progress Report No. 1, January 15, 1960.

2. Schapery, R. A., Stimpson, L. D., and Williams, M. L.: "Fundamental Studies Relating to Systems Analysis of Solid Propellants", California Institute of Technology GALCIT 101, Progress Report No. 2, April 15, 1959.

3. Schapery, R. A., Stimpson, L. D., and Williams, M. L.: "Fundamental Studies Relating to Systems Analysis of Solid Propellants", California Institute of Technology, GALCIT 101 Progress Report No. 3, July 15, 1959.

4. Blatz, P. J., Schapery, R. A., Stimpson, L. D., and Williams, M. L.: "Fundamental Studies Relating to Systems Analysis of Solid Propellants", California Institute of Technology GALCIT 101 Progress Report No. 4, October 15, 1959.

5. Blatz, P. J., Knauss, W. G., Schapery, R. A., Stimpson, L. D., and Williams, M. L.: "Fundamental Studies Relating to Systems Analysis of Solid Propellants", California Institute of Technology GALCIT 101 Progress Report No. 5, January 15, 1960.

6a. Nadai, A.: "Theory of Flow and Fracture of Solids", p. 175, McGraw-Hill, 1950.

6b. Orowan, E.: Progress in Physics, Vol. 12, p. 185, 1949.

7. Mises, R. V.: Die Differential and Integral-Gleishunger der Mechanik and Physik, Vol. 2, p. 605, 1927.

8. Hencky, H., and Angew, Z.: Math Mechanick, Vol. 4, p. 323, 1924.

9. Haigh, B. P.: Engineering, Vol. 190, p. 158, 1920.

10. Rivlin, R. S.: Philosophical Transactions, A 240, pp. 459, 491, 509, 1948.

11. Treloar, L. R.: Physics of Rubber Elasticity, 2, Oxford, 1953.

12. Martin, G. M., Roth, F. L., and Stiehler, R. D.: Journal of Research of the National Bureau of Standards, December 1958.

13. Treloar, L. R.: Physics of Rubber Elasticity, Chapter IV, 1953.

14. Jaeger, J. C.: "Elasticity Fracture and Flow", p. 65, Methuen 1956.

15. Green, Zerna: Theoretical Elasticity, Chapter V, Oxford, 1956.

16. Ferry, W., Landel, R., and Williams, M. L.: Journal of American Chemical Society, Vol. 77, p. 370, 1950.

17. Brettschneider, H. and Dale, W.: "Experience with the Alinco High Rate Tensile Tester", Bulletin of Seventeenth Meeting of JANAF Physical Properties Panel, p. 43, May 1958.

18. Jones, J.: "Tensile Testing of Elastomers at Ultra High Strain Rates", Presented at High Rate Symposium, Boston, Massachusetts, January 1960.

19. Gent, A. N. and Lindley, P. B.: "Compression of Bonded Rubber Blocks", Publication No. 324, Journal of British Rubber Producer's Association, Vol. 173, p. 111, 1959.

20. Gent, A. N. and Lindley, P. B.: "Internal Rupture of Bonded Rubber Cylinder in Tension", Proceedings Royal Society, A. Vol. 249, p. 195, 1959.

21. Dowler, W., Lewis, G., and Stimpson, L. D.: Bulletin of Eighteenth Meeting of JANAF Physical Properties Panel, p. 27, June 1959.

22. Bergen, N., Messersmith, W. and Rivlin, R. S.: "The Stress Relation for Biaxial Deformation of Filled High-Polymers", Armstrong Cork Company and Brown University, 1959. Presented at Annual ASME Meeting in New York City, December 1959.

23. Ordahl, D. D.: "Burst Tests on Solid Propellants" (NOTS Burst Test), Bulletin of Eighth Meeting of JANAF Physical Properties Panel, p. 7, July 1953.

24. Shank, M. E.: Private communication.

25. McCullough, J.: "Studies on Velocity of Crack Propagation", Internal Report to Chemistry Department, Thiokol Chemical Corporation, Redstone Division, Huntsville, Alabama, Sept. 1959.

26. Ang, D. D. and Williams, M. L.: "Combined Stresses in an Orthotropic Plate Having a Finite Crack", GALCIT SM 60-1, Guggenheim Aeronautical Laboratory, California Institute of Technology.

27. Williams, M. L.: "On the Stress Distribution at the Base of a Stationary Crack", Journal of Applied Mechanics, March 1957.

28. Chapkis, R. L. and Williams, M. L.: "Stress Singularities for a Sharp-Notched Polarly Orthotropic Plate., Proceedings Third National Congress Applied Mechanics, June 1958.

29. Higuchi, M.: "On the Splitting Stress Produced in a Wooden Log Subjected to a Lateral Force", Japanese Institute of Applied Mechanics, Report No. 6, March 1955.

30. Blatz, P. J.: "Finite Deformation Analysis of a Circular Log Split by a Wedge", GALCIT SM 60-9, Guggenheim Aeronautical Laboratory, California Institute of Technology.

31. Gross, B.: "Mathematical Structure of Theories of Visco-elasticity", Hermann 1953.

DISTRIBUTION LIST

Galcit 101

GOVERNMENT AGENCIES

Advanced Research Projects Agency
Washington 25, D. C.
Attn: Mr. John Kincaid (1)

National Aeronautics and Space Administration
1512"H" Street, N. W.
Washington 25, D. C.
Attn: Mr. Elliott Mitchell (1)

National Aeronautics and Space Administration
Lewis Research Center
21000 Brookpark Road
Cleveland 35, Ohio
Attn: Mr. George Mandel (1)

Office of the Department of Defense, Research and Engineering
Pentagon Building, Room 3E1030
Washington, D. C.
Attn: Mr. William E. Sheehan (1)

Solid Propellant Information Agency
The Johns Hopkins University
Applied Physics Laboratory
8621 Georgia Avenue
Silver Springs, Maryland
Attn: Mr. M. T. Lyons (3)

ARMY

Aberdeen Proving Ground
Internal Ballistics Laboratory
Aberdeen, Maryland
Attn: Dr. John H. Frazer, Chief (1)

Office of Ordnance Research
Box C-M, Duke Station
Durham, North Carolina
Attn: Dr. James Murray (1)

Piccatiny Arsenal
Dover, New Jersey
Attn: Miss E. MacAbee (1)

Redstone Arsenal
Army Rocket and Guided Missile Agency
Huntsville, Alabama
Attn: Mr. Thomas H. Duerr (1)

NAVY

Mechanics Branch
Office of Naval Research
Washington 25, D. C.
Attn: Dr. Harold Liebowitz (1)

Special Projects Group
Bureau of Naval Weapons
Washington 25, D. C.
Attn: Mr. William Cohen (1)

U. S. Navy Ordnance Test Station
Propulsion Development Department
China Lake, California
Attn: Mr. Douglas D. Ordahl:Code 45 (1)

AIR FORCE

Air Force Ballistic Missile Development
Solid Propellant Branch
Air Force Unit Post Office
Los Angeles 45, California
Attn: Major Ralph Harned (1)

Air Research and Development Command
European Office
Library, Technical Information Office
Shell Building 47, Rue Canterstein
Brussels, Belgium
Attn: Miss Margaret P. Papesch (1)

Flight Test Rocket Development Station
Propulsion Section
Edwards Air Force Base
Muroc, California
Attn: Mr. D. A. Hart (1)
Attn: Mr. Tom Davidson (1)

Office of Scientific Research
Washington 25, D. C.
Attn: Mr. Milton Rogers (1)

Space Technology Laboratories
Solid Propellant Branch
Department of Propulsion Laboratory
5740 Arbor Vitae
Los Angeles, California
Attn: Mr. Robert Anderson (1)

Wright Air Development Division
Aeronautical Research Laboratory
Wright-Patterson Air Force Base
Dayton, Ohio
Attn: Mr. Richard B. Baird (1)

UNIVERSITIES

Brown University
Department of Applied Mathematics
Providence 12, Rhode Island
Attn: Dr. E. H. Lee (1)

California Institute of Technology
Pasadena, California
Attn: GALCIT Library (2)
Attn: JPL Library (2)

Columbia University
Department of Civil Engineering
New York 27, New York
Attn: Dr. A. M. Freudenthal (1)

Massachusetts Institute of Technology
Department of Mechanical Engineering
Cambridge 39, Massachusetts
Attn: Dr. M. E. Shank (1)

New York University
College of Engineering
New York 53, New York
Attn: Dr. George Gerard (1)
Attn: Dr. Bernard W. Shaffer (1)

Polytechnic Institute of Brooklyn
Department of Aeronautical Engineering
Brooklyn, New York
Attn: Dr. Radok (1)
Attn: Prof. F. Pohle (1)

Purdue University
Lafayette, Indiana
Attn: Library (1)

University of Alabama
College of Engineering
University, Alabama
Attn: Dr. William D. Jordan (1)

University of California
Department of Civil Engineering
Berkeley 4, California
Attn: Prof. Karl S. Pister (1)

INDUSTRIES

Thiokol Chemical Corporation
Redstone Division
Huntsville, Alabama
Attn: Mr. James P. Lutz (6)
Attn: Mr. John S. Wise (2)

Thiokol Chemical Corporation
Elkton Division
Elkton, Maryland
Attn: Mr. Ernest Sizemore (2)

Thiokol Chemical Corporation
Utah Division
Brigham City, Utah
Attn: Mr. C. S. Roberts, Jr. (2)
Attn: Mr. John Bruggeman (1)

Thiokol Chemical Corporation
Hunter-Bristol Division
Bristol, Pennsylvania
Attn: Mr. Don Mueller (2)

Aerojet-General Corporation
Solid Propellant Rocket Plant
Sacramento, California
Attn: Mr. John Billheimer (1)
Attn: Mr. A. Fraser (1)
Attn: Dr. James H. Wiegand (1)
Attn: Technical Library (1)

Aerojet-General Corporation
P. O. Box 296
Azusa, California
Attn: Mr. William Cox (1)
Attn: Mr. Kenneth Bills (1)

Astrodyne, Inc.
P. O. Box 548
McGregor, Texas
Attn: Mr. S. C. Britton (1)
Attn: Mr. C. C. Dugger (1)

Rocketdyne
6633 Canoga Avenue
Canoga Park, California
Attn: Mr. Frank Cramer (1)

INDUSTRIES (cont'd)

Grand Central Rocket Co.
P. O. Box 111
Redlands, California
Attn: Mr. J. E. Fitzgerald (2)

Olin Mathieson Chemical Corporation
Internal Ballistics Section
Box 508
Marion, Illinois
Attn: Mr. Robert W. Ziem (1)

Boeing Airplane Company
P. O. Box 3707
Seattle, Washington
Attn: Mr. Len Hadlock (1)

Douglas Aircraft Company, Inc.
3000 Ocean Park Boulevard
Santa Monica, California
Attn: Engineering Library
Department A-260 (1)

Hughes Aircraft Company
Systems Development Laboratories
Culver City, California
Attn: Mr. Norman Au (1)

Hercules Powder Company
Allegheny Ballistics Laboratory
Cumberland, Maryland
Attn: Mr. Ross H. Petty - Library (2)
Attn: Mr. James H. Thacher (1)

Poulter Laboratories
Stanford Research Institute
Menlo Park, California
Attn: Dr. T. L. Smith (1)
Attn: Mr. W. L. Dowler (1)

Rocket Power/Talco
Falcon Field
Mesa, Arizona
Attn: Library (1)

Lockheed Aircraft Corporation
Georgia Division
Marietta, Georgia
Attn: Sci-Information Center (1)

INDUSTRIES (cont'd)

Lockheed Aircraft Corporation
Missile Systems Division
Sunnyvale, California
Attn: Library (1)

SWEDEN

Research Institute of National Defense
Stockholm Sweden
Attn: G. Lennart Magnusson (1)

GALCIT

Internal Distribution (10)

File (3)